

# A comprehensive model for stability of dispersed oil-water flow in horizontal and inclined pipes



Luciano D. Paolinelli\*

Institute for Corrosion and Multiphase Technology, Department of Chemical & Biomolecular Engineering, Ohio University, Athens, OH 45701, USA

## HIGHLIGHTS

- A mechanistic model for stability of liquid-liquid flow in pipes is proposed.
- It accounts for break-up, sedimentation, dispersion and accumulation of droplets.
- Droplet coalescence and segregation are considered by attaining critical accumulation.
- Critical droplet accumulation is associated to the phase inversion point.
- Model predictions agree well with numerous sets of experimental data.

## ARTICLE INFO

### Article history:

Received 10 August 2019  
 Received in revised form 5 October 2019  
 Accepted 28 October 2019  
 Available online 30 October 2019

### Keywords:

Dispersed flow  
 Liquid-liquid  
 Pipes  
 Stability bounds  
 Droplet accumulation  
 Modeling

## ABSTRACT

Prediction of dispersed flow regimes in liquid-liquid pipe flow is of great importance for many industrial processes. This work proposes a mechanistic model to determine the stability bounds of dispersed liquid-liquid flow patterns that presents significant improvements compared to other classical criteria. The model accounts for turbulent break-up of dispersed phase droplets, sedimentation, dispersion, and accumulation of droplets. In addition, droplet coalescence and segregation are considered by means of attaining critical concentrations that can be associated with the phase inversion point of the liquid-liquid mixture. Modeled bounds are compared with available experimental data, showing good agreement in flows of mineral oil and water, as well as flows of crude oil and water. Moreover, the model is more accurate and descriptive than other predictions from commonly used criteria. The effect of fluid properties, flow rates, and pipe geometry are discussed. Limitations and possible refinements of the suggested model are also treated.

© 2019 Elsevier Ltd. All rights reserved.

## 1. Introduction

The simultaneous flow of two immiscible liquids in horizontal and inclined pipes can produce a variety of flow patterns. These various flow regimes can be characterized according to the spatial distribution of both fluids in the pipe as well as at their interface. The ability to predict the occurrence of different flow regimes is of paramount importance in industrial processes in which, for example, friction losses, heat and mass transfer, and chemical/electrochemical reactions are involved.

In the case of the flow of water and less dense liquid hydrocarbons of relatively low viscosity (e.g., <100 mPa-s), the existence of several types of flow regimes in horizontal pipes has been reported

(Angeli and Hewitt, 2000b; Elseth, 2001; Lovick and Angeli, 2004; Nädler and Mewes, 1997; Trallero, 1995). One of the most popular classifications of flow patterns is the one made by Trallero (1995) consisting of six types of flow configurations:

- Stratified flow (ST): The two immiscible liquids flow as separated layers. The water, which is usually heavier, flows at the pipe bottom and the oil on top, with a smooth or wavy interface between both phases. The velocities of the fluids are usually low.
- Stratified flow with mixing at the interface (ST & MI): The interface between both fluids becomes unstable producing some mixing of droplets and/or globules of each liquid into the other. However, the liquids still flow as two separated layers. The velocities of the fluids are higher than in the case of the ST flow pattern.
- Dual dispersion – oil in water and water in oil (D O/W & D W/O): The two fluids are distributed along the entire pipe cross-section. The water flows as the continuous phase (with

\* Address: Institute for Corrosion and Multiphase Technology, Department of Chemical & Biomolecular Engineering, Ohio University, 342 W. State Street, Athens, OH 45701, USA.

E-mail address: [paolinel@ohio.edu](mailto:paolinel@ohio.edu)

dispersed oil droplets) at the lower half of the pipe, and the oil flows as the continuous phase (with dispersed water droplets) at the upper half of the pipe.

- Dispersion of oil in water with a water layer (D O/W & W): The water is the continuous phase at the entire pipe cross-section. However, oil droplets (usually less dense than water) flow mostly gathered at the upper half of the pipe, and the pipe bottom shows only water.
- Dispersion of water in oil (D W/O): The oil is the continuous phase with dispersed water droplets distributed across the pipe cross-section.
- Dispersion of oil in water (D O/W): The water is the continuous phase with dispersed oil droplets distributed in the pipe cross-section more evenly than in the case of the D O/W & W flow pattern.

The determination of the operating conditions (e.g., flow rates of oil and water) where flow pattern is no longer stratified and/or stratified with mixing at the interface has been the focus of numerous studies, mainly due to the significant changes in friction losses and heat transfer associated with a layered co-current flow compared to an oil or water continuous flow. The most accepted stratified to non-stratified flow transition criteria comes from the analysis of the stability of the stratified oil-water interface made from momentum equations evaluated over a control volume of each flowing layer of oil and water (Al-Wahaibi and Angeli, 2007; Brauner and Moalem Maron, 1992; Torres et al., 2015).

The prediction of the transition from dispersed flow (oil or water as continuous at the entire pipe cross-section) to semi-dispersed flow (be it dual dispersion and/or stratified flow with mixed interface), which is the focus of the present study, is also very important. This is not only due to friction losses and heat or mass transfer alteration but also due to, for example, chemical and/or electrochemical reactions that may occur between the chemical components of the liquids and the pipe wall. A known example of this is corrosion of carbon steel pipes in oil production and transportation lines. If produced water containing corrosive gases such as CO<sub>2</sub> and H<sub>2</sub>S segregates from dispersion in crude oil and contacts the pipe wall (phenomenon referred to as water wetting), steel can be oxidatively dissolved at high rates, thereby seriously compromising pipe integrity (NACE, 2008; Pots et al., 2006). Several studies have been devoted to understanding and predicting the transition from dispersed to semi-dispersed or stratified regimes in liquid-liquid pipe flow (Amundsen, 2011; Brauner, 2001; Sharma et al., 2011; Trallero, 1995; Valle, 2000; Zhang and Sarica, 2006).

Trallero (1995) suggested that after a phase is dispersed, it will not form a segregated layer unless the kinetic energy supplied by the motion of the continuous phase falls below a certain threshold where droplets start to coalesce due to the action of gravity. Consequently, he proposed a balance between the gravity ( $F_g$ ) and turbulent ( $F_t$ ) forces on droplets along the normal direction to the pipe wall as a criterion to predict the dispersed flow pattern transition:

$$F_g = \frac{1}{6} \pi d^3 |\rho_d - \rho_c| g \cos \beta \quad (1)$$

$$F_t = \frac{1}{8} \rho_c \pi d^2 v'^2 \quad (2)$$

where  $d$  is the diameter of a dispersed droplet,  $g$  is the gravitational constant,  $\beta$  is the inclination angle of the pipe,  $v'$  is the r.m.s. value of the turbulent velocity fluctuations in the radial direction of the pipe, and  $\rho_c$  and  $\rho_d$  are the densities of the continuous and dispersed phases, respectively. It is worth mentioning that the drag

force in Eq. (2) assumes a drag coefficient of value 1. Then dispersed droplets will remain suspended if:

$$F_t > F_g \quad (3)$$

As can be noticed from Eqs. (1) and (2), the assessment of gravity and turbulent forces depends on the droplet size ( $d$ ) and the r.m.s. value of turbulent velocity fluctuations ( $v'$ ). Both variables depend on the specific location of the pipe where this assessment is attempted. Moreover, droplet sizes in dispersed turbulent pipe flow vary widely and can follow distributions such as log-normal or Rosin-Rammler (Angeli and Hewitt, 2000a; Karabelas, 1978; Paolinelli et al., 2018; Simmons and Azzopardi, 2001). However, it is noteworthy that if the expression (3) is evaluated for the maximum droplet size ( $d_{\max}$ ), the criterion will be also fulfilled for all the other smaller droplet sizes.

The Lagrangian approach described above was also suggested by Brauner (2001) as one of the criteria needed to assure the stability of dispersed flow in pipes. She proposed a critical droplet size from the balance  $F_t = F_g$ :

$$d_{cb} = \frac{3}{4} \frac{\rho_c v'^2}{|\rho_d - \rho_c| g \cos \beta} \quad (4)$$

where  $v'$  is approximated as the friction velocity:

$$u^* = \sqrt{\frac{\rho_m f}{2 \rho_c}} U_c \cong \sqrt{\frac{f}{2}} U_c \quad (5)$$

where  $f$  is the Fanning friction factor,  $\rho_m$  is the density of the liquid mixture, and  $U_c$  is the velocity of the continuous phase. Then, Eq. (4) leads to:

$$d_{cb} = \frac{3}{8} \frac{\rho_c f U_c^2}{|\rho_d - \rho_c| g \cos \beta} \quad (6)$$

Brauner suggested that  $d_{cb}$  is the maximum droplet size above which migration of droplets towards the pipe walls occurs due to buoyant forces. She also introduced another criterion for critical droplet size suggested by Barnea (1987):

$$d_{c\sigma} = \left[ \frac{0.4\sigma}{|\rho_d - \rho_c| g \cos \beta'} \right]^{1/2} \quad (7)$$

$$\beta' = \begin{cases} |\beta|, & |\beta| < 45^\circ \\ 90 - |\beta|, & |\beta| > 45^\circ \end{cases} \quad (8)$$

where  $\sigma$  is the interfacial tension between both liquids. The critical droplet size  $d_{c\sigma}$  represents the maximum droplet diameter above which droplets become significantly deformed mainly due to gravity. It is worth mentioning that Eq. (7) is based on an expression reported by Brodkey (1967) that estimates when drag forces on droplets deviate from spherical behavior due to shape distortion, producing swerving motions.

Subsequently, the critical droplet size is estimated as:

$$d_{crit} = \text{Min}(d_{cb}, d_{c\sigma}) \quad (9)$$

and dispersed flow is stable when the continuous phase flow is turbulent enough to disrupt the dispersed phase into droplets smaller than the critical size:

$$d_{\max} \leq d_{crit} \quad (10)$$

provided that the continuous phase flow is turbulent  $Re_c \geq 2100$ , where  $Re_c = \rho_c D U_c / \mu_c$ ,  $D$  is the pipe internal diameter, and  $\mu_c$  is the viscosity of the continuous phase.

Brauner stated that expression (10), which involves the criteria expressed in Eqs. (6) and (7), comprises a complete assessment of the stability of dispersed flow, where spherical non-deformed

droplets are produced ( $d_{\max} < d_{c\sigma}$ ) and excessive accumulation of droplets at the bottom or top of the pipe (referred to as “creaming”) is hampered ( $d_{\max} < d_{cb}$ ). Other authors (Torres et al., 2015) suggested that the criterion  $d_{\max} \leq d_{c\sigma}$  defines the transition to semi-dispersed flow, and the criterion  $d_{\max} \leq d_{cb}$  represents the transition to fully dispersed flow.

Although the criteria mentioned above for assessing dispersed flow are relatively simple and have been used as part of several suggested models for flow pattern prediction in oil-water pipe flow (Brauner, 2001; Sarica and Zhang, 2008; Torres et al., 2015; Trallero, 1995; Wang et al., 2017), they are open to question since the complexity of liquid-liquid dispersed flow is far from being well described with such Lagrangian perspectives. Some of the main drawbacks of these criteria are:

- Turbulent dispersive forces produced by the velocity fluctuations in the continuous phase flow tend to homogenize the concentration of dispersed droplets across the pipe cross-section (Karabelas, 1977; Segev, 1984). Therefore, if droplets tend to accumulate at the pipe walls due to gravity forces, the dispersive turbulent forces will mainly tend to eject droplets towards the pipe core, as assumed by expression (3) and criterion  $d_{\max} \leq d_{cb}$ . However, the fulfillment of this criterion does not assure that dispersed droplets will not intermittently contact the pipe wall since the occurrence and direction of turbulent forces is stochastic in nature.
- The concept of migration of dispersed droplets towards the pipe wall and their excessive accumulation (“creaming”) cannot be contemplated by the simple balance between gravity and turbulent forces on the largest droplets (expression (3) and criterion  $d_{\max} \leq d_{cb}$ ), since it is not possible to estimate the actual concentration of dispersed droplets across the pipe section. The knowledge of the actual concentration of dispersed droplets at critical locations such as the bottom or the top of the pipe is crucial in order to assess if dispersed phase coalescence or phase inversion will occur (Amundsen, 2011; Kroes et al., 2013; Paolinelli et al., 2018; Pots et al., 2006; Valle, 2000).
- The assessment of the existence of significantly deformed droplets via the criterion  $d_{\max} < d_{c\sigma}$  does not necessarily imply that droplet coalescence will occur. The rate of coalescence between dispersed droplets mainly depends on how frequently they collide with each other, among other important factors such as collision time, energy, physicochemical characteristics of the liquid-liquid interface, etc., as described elsewhere (Liao and Lucas, 2010). In this regard, the local concentration of dispersed droplets plays a very important role on coalescence rate. Particularly, when a certain critical droplet concentration is achieved, coalescence becomes dominant (Arashmid and Jeffreys, 1980; Liao and Lucas, 2010). Again, neither the criterion  $d_{\max} < d_{c\sigma}$  nor  $d_{\max} \leq d_{cb}$  account for the estimation of dispersed droplet concentration at the pipe cross-section.

Other approaches have also been proposed to determine the transition between dispersed and semi-dispersed flow. Zhang and Sarica (2006) suggested that the transition to a dispersed regime in oil-water pipe flow can be predicted using a model previously developed to estimate gas-void fraction in slug body in liquid-gas pipe flow (Zhang et al., 2003). The model is based on the balance between the total turbulent kinetic energy and total surface energy of the system. Even though this approach agrees somewhat well with select experimental data, the model is too simplistic since it does not account for the effect of sedimentation of dispersed droplets and their concentration across the pipe section. Sharma et al. (2011) introduced a model based on the concept that oil-water flow structures stabilize where the total energy of the system is at its minimum. They considered the potential energy, kinetic energy and

surface energy of the of the oil and water phases. To assess full dispersion of water in oil or oil in water, the kinetic and surface energies are minimized and a closure criteria to assure feasibility of dispersed flow is used, which is that the holdup represented by the area of the maximum droplet size over the pipe cross-section must be smaller or equal to the phase inversion point. Although the model results in terms of dispersed flow pattern prediction somewhat followed the trend of some experimental data, the authors pointed out that occurrence of the dispersed flow pattern was overpredicted due to the use of conservative criteria for the onset of entrainment.

Valle (2000) proposed a more comprehensive model to estimate flow characteristics of dispersed oil-water flow considering the effect of the distribution of dispersed droplets across the pipe section on the local density and viscosity of the mixture flow and its impact on the flow velocity profile and pressure drop. A two-dimensional transport model was used to characterize the effect of droplet convection due to gravity and other flow forces, such as Saffman type near pipe wall, as well as the dispersive effect of the continuous phase turbulence. Regardless, the use of this comprehensive model to estimate flow characteristics and local droplet concentration, the prediction of dispersed flow pattern was achieved by employing a mass balance that considered co-flowing layers of each phase with simultaneous droplet entrainment and deposition through their interface in which full dispersion is achieved when one phase is completely entrained into the other. This flow pattern transition model requires different calibration coefficients to describe the behavior of water and oil droplets in different systems, which makes it difficult to use and prone to inaccuracy for general applications. Amundsen (2011) used a transport model to determine the *in situ* fractions of a dispersed phase across the pipe section in dispersed oil-water flow environments. The model considered sedimentation of dispersed droplets due to gravity and droplet dispersion due to the turbulence of the continuous phase. The author estimated the occurrence of a fully dispersed flow pattern when the largest volumetric fraction of the dispersed phase across the pipe section was lower than the phase inversion point. This approach has been an improvement compared to the simpler criteria involved in Eq. (10). However, modeled results were not completely in line with the experimental data, possibly due to underprediction of the turbulent diffusivity term in the proposed transport model. Moreover, no extensive comparisons with available experimental data were performed.

The aim of this study is to introduce a more comprehensive model to assess the stability bounds for turbulent dispersed liquid-liquid flow in horizontal and inclined pipes, where only one phase remains as continuous across the entire pipe section. The model is mainly based on the computation of critical accumulation of dispersed droplets at either the bottom or the top of the pipe depending on whether the dispersed phase is heavier or lighter, respectively. This model includes the effect of the continuous phase turbulence on turbulent break-up of dispersed phase droplets, as well as the convection of dispersed droplets due to gravity and the dispersive effect of the continuous phase turbulence by using an Eulerian approach with an advection-diffusion formulation. The effect of the physicochemical properties and flow rates of the fluids as well as pipe geometry (e.g., diameter, inclination) are assessed and discussed. The model is compared with extensive sets of available experimental data for mineral oil and water, and crude oil and water flows; as well as with predictions from other available criteria.

## 2. Description of the proposed model

### 2.1. Main criterion

Turbulent liquid-liquid dispersed flow can remain stable, without showing major segregation of a dispersed phase, provided that

the concentration of dispersed phase droplets at any location of the pipe cross-section do not exceed a critical value ( $C_{crit}$ ) at which significant coalescence and separation of the dispersed phase is unavoidable. As mentioned above, the most critical locations for droplet accumulation are the bottom or the top of the pipe depending on whether the dispersed phase is denser than the continuous phase or not. Therefore, the criterion can be written as follows:

$$C_{b,t} < C_{crit} \quad (11)$$

where  $C_{b,t}$  is the concentration of dispersed phase droplets either at the bottom or the top of the pipe, whichever applies.

The determination of the critical concentration of the dispersed phase is strongly dependent on the characteristics of the studied liquid-liquid system. Depending on the physicochemical properties of the immiscible liquids (e.g., density, viscosity, interfacial tension) as well as their content of surface active compounds, liquid-liquid dispersions can be more or less prone to coalesce and segregate. Irrespective of this behavior, there is a critical concentration or holdup of one dispersed liquid into the other where the dispersed phase is no longer stable as dispersed droplets and spontaneously turns to be the continuous phase, incorporating the former continuous phase as a dispersed phase. This critical dispersed phase holdup is termed the phase inversion point. The inversion point may not pertain to a single value, and may involve a concentration region where both liquid phases can remain as dispersed and continuous at the same time forming complex inhomogeneous dispersions, which are called ambivalent (Arashmid and Jeffreys, 1980; Brauner and Ullmann, 2002; Ioannou et al., 2005; Piela et al., 2008; Selker and Sleicher Jr., 1965). Regardless of the complexity of the phase inversion phenomenon, it can be inferred that if a given liquid-liquid dispersion accumulates dispersed phase concentrations similar to the phase inversion point, local coalescence of the dispersed phase is to be expected along with its segregation; and consequently, dispersed flow will no longer be stable. Therefore, during the remainder of this work the critical concentration of the dispersed phase to avoid segregation ( $C_{crit}$ ) will be associated with the inversion point (*IP*) of the studied liquid-liquid systems. Then, expression (11) leads to:

$$C_{b,t} < IP \quad (12)$$

The expression above implies that dispersed phase droplets are mostly controlled by turbulent breakup and their coalescence is not dominant unless a concentration similar to the inversion point is reached.

## 2.2. Calculation of the concentration of dispersed droplets

The concentration of dispersed phase droplets across the pipe section can be approximated using an advection-diffusion model. Assuming that the liquid-liquid flow is already dispersed and at steady state, and the droplet concentration only varies with the pipe vertical direction ( $y$ ), the balance between the fluxes of settling and dispersed droplets as well as the continuous phase flux leads to the following equation (Karabelas, 1977):

$$U_{s,y}C(1 - C) - \varepsilon \frac{\partial C}{\partial y} = 0 \quad (13)$$

$$U_{s,y} = U_s \cos \beta \quad (14)$$

where  $C$  is the volumetric concentration of dispersed droplets,  $\varepsilon$  is the droplet turbulent diffusivity that is assumed to be constant across the pipe section,  $U_s$  is the settling velocity of the mean dispersed droplet size, and  $y$  is the vertical coordinate with respect to the pipe direction. Eq. (13) neglects the effect of hydrodynamic forces near the pipe wall such as Saffman type forces and lubrication forces. It is assumed that no dispersed droplet mass is lost at

the wall due to droplet sticking; thus, the total droplet mass remains constant across the pipe section:

$$\int C(y)dA = \varepsilon_d A \quad (15)$$

where  $A$  is the pipe cross-section and  $\varepsilon_d$  is the mean volumetric fraction or holdup of dispersed phase, which assuming no slip between the dispersed and the continuous phases is:

$$\varepsilon_d = \frac{U_{sd}}{U_{sd} + U_{sc}} \quad (16)$$

where  $U_{sd}$  is the superficial velocity of the dispersed phase, and  $U_{sc}$  is the superficial velocity of the continuous phase.

From previous work (Paolinelli et al., 2018), it is known that dispersed droplets can effectively stick and spread on the pipe wall if pipe wettability is favorable, forming very thin segregated liquid layers or rivulets of <1 mm thickness. These thin layers are neglected in the present analysis since they do not represent a case of major segregation where the stability of dispersed flow is significantly compromised.

The droplet turbulent diffusivity in Eq. (13) is calculated as:

$$\varepsilon = \zeta \frac{D}{2} u^* = \zeta \frac{D}{2} \sqrt{\frac{\rho_m f}{2\rho_c}} U_c \quad (17)$$

where  $\zeta$  is the dimensionless eddy diffusivity that can be considered as constant with a value of 0.255 (Karabelas, 1977). Since fully dispersed flow and no slip between phases are assumed, the continuous phase velocity is considered similar to the mixture velocity  $U_c \cong U_m$ , which is by definition the sum of  $U_{sd}$  and  $U_{sc}$ . The Fanning friction factor for turbulent flow in a hydraulically smooth pipe can be calculated using the Blasius correlation:

$$f = 0.046 Re_m^{-0.2} \quad (18)$$

where  $Re_m = \rho_m D U_m / \mu_m$ . In cases where the internal roughness of the pipe surface is considerable, explicit approximations of the Colebrook formula such as the one provided by Haaland (1983), can be used to calculate friction factor:

$$f = \left\{ -3.6 \log \left[ \frac{6.9}{Re_m} + \left( \frac{e_r}{3.75D} \right)^{1.11} \right] \right\}^{-2} \quad (19)$$

where  $e_r$  is the equivalent sand roughness of the internal pipe wall.

The density of the liquid-liquid mixture is estimated as:

$$\rho_m = \varepsilon_d \rho_d + (1 - \varepsilon_d) \rho_c \quad (20)$$

and the mixture viscosity ( $\mu_m$ ) is considered similar to the continuous phase viscosity ( $\mu_m \cong \mu_c$ ), based on pressure drop experimental results in dispersed flow of mineral oil and water in pipes (Elseth, 2001; Lovick and Angeli, 2004; Trallero, 1995). However, pressure drop of dispersed liquid-liquid flow can be significantly higher than predicted considering  $\mu_m \cong \mu_c$ ; particularly, when mixture velocities are high and dispersed phase holdup is close to the phase inversion point (Angeli and Hewitt, 1999). This behavior is also common in crude oil and water flows in pipes (Kroes et al., 2013; Valle, 2000) in which tight dispersions or emulsions can be formed and the apparent viscosity of the mixture increases (Plasencia et al., 2013; Valle, 2000).

The settling velocity of the mean dispersed droplet size ( $\bar{d}$ ) in Eq. (14) is calculated as follows:

$$U_s = \sqrt{\frac{4 \bar{d} |\rho_d - \rho_c| g}{3 \rho_c C_D}} \quad (21)$$

where  $C_D$  is the droplet drag coefficient that is approximated with the Schiller-Naumann correlation (solid spheres) (Schiller and Naumann, 1933):

$$C_D = \frac{24}{Re_p} \left(1 + 0.15 Re_p^{0.687}\right) \quad (22)$$

where  $Re_p = \rho_c \bar{d} U_s / \mu_c$ , with  $Re_p < 1000$ .

Although Eq. (13) was developed and validated for dilute dispersions, it has successfully been used to predict the concentration profile of dispersed particles in liquid pipe flow with volume concentrations as high as 20% (Kaushal et al., 2002).

Eq. (13) and its mass conservation constraint (15) have a closed-form solution suggested by Karabelas (1977):

$$C(y) = \left[1 + 2 \frac{(1 - \varepsilon_d)}{\varepsilon_d} \frac{I_1(K)}{K} \exp\left[s_d K \left(\frac{2y}{D} - 1\right)\right]\right]^{-1} \quad (23)$$

$y = 0$  and  $y = D$  at the bottom and top of the pipe respectively. Where:

$$K = \frac{DU_{s,y}}{2\varepsilon} \quad (24)$$

$I_1(K)$  is the modified Bessel function of order 1 (truncated at the sixth term):

$$I_1(K) = \frac{1}{2}K \left[1 + \frac{K^2}{8} + \frac{K^4}{192} + \frac{K^6}{9216} + \frac{K^8}{737280} + \frac{K^{10}}{88473600}\right] \quad (25)$$

and  $s_d$  is an integer variable:

$$s_d = \begin{cases} 1 & \rho_d > \rho_c \\ -1 & \rho_d < \rho_c \end{cases} \quad (26)$$

Finally, the concentration of dispersed phase droplets at the bottom or the top of the pipe is:

$$C_{b,t} = \left[1 + 2 \frac{(1 - \varepsilon_d)}{\varepsilon_d} \frac{I_1(K)}{K} \exp(-K)\right]^{-1} \quad (27)$$

The use of the Bessel function in (25) may be limited for relatively high values of the parameter  $K$  as discussed elsewhere (Paolinelli et al., 2018).

Consequently, the criterion in (11) and (12) can be easily implemented solving simultaneously for the settling velocity of dispersed droplets (Eq. (21)) and droplet concentration using the close-form solution given in (27).

### 2.3. Calculation of the size of dispersed droplets

It is assumed that the main mechanism that controls the size of dispersed water droplets is turbulent break-up. A comprehensive and accurate description of the effect of the continuous phase turbulence on the size of dispersed phase droplets produced along a pipe would require the use of methods such as population balance where realistic break-up frequencies and daughter droplet size probability functions are assessed to obtain droplet size distribution. However, Kostoglou and Karabelas (2005) demonstrated that mean droplet sizes computed from population balance are proportional to the simple expression proposed by Hinze (1955):

$$d_{\max,o} = 0.725 \left(\frac{\sigma}{\rho_c}\right)^{3/5} \varepsilon^{-2/5} \quad (28)$$

where  $d_{\max,o}$  is the maximum droplet size in dilute dispersion, and  $\varepsilon$  is the mean energy dissipation rate in the continuous phase flow:

$$\varepsilon = \frac{2\rho_m f U_c^3}{D\rho_c(1 - \varepsilon_d)} \quad (29)$$

Brauner (2001) proposed the following expression for dense dispersions based on the assumption that as coalescence takes place in dense systems, the incoming flow of the continuous phase

should carry enough turbulent energy to disrupt the tendency to coalesce and disperse the other phase:

$$d_{\max,\varepsilon_d} = \left(6C_H \frac{\varepsilon_d}{(1 - \varepsilon_d)}\right)^{3/5} \left(\frac{\sigma}{\rho_c}\right)^{3/5} \varepsilon^{-2/5} \quad (30)$$

where  $C_H$  is a constant of order 1. Eq. (30) is not directly used in the current model, and is only included to show the droplet size formulation used by the Brauner's dispersion model (Eq. (10),  $d_{\max} = \text{Max}(d_{\max,o}, d_{\max,\varepsilon_d})$ ), which is compared against experimental data in a further section. Instead, to account for the effect of the volumetric fraction of dispersed phase on maximum droplet size, the size  $d_{\max,o}$  is altered by the factor suggested by Mlynek and Resnick (1972), which describes fairly well experimental data from various liquid-liquid systems:

$$d_{\max} = d_{\max,o} (1 + C_{\varepsilon_d} \varepsilon_d) \quad (31)$$

where  $C_{\varepsilon_d}$  is a parameter that varies with the dispersed phase fraction:

$$C_{\varepsilon_d} = \begin{cases} 5.4 & \varepsilon_d \leq 0.2 \\ \sim 3 & \varepsilon_d > 0.2 \end{cases} \quad (32)$$

Eq. (31) is valid provided that (Brauner, 2001; Kubie and Gardner, 1977):

$$\left(\frac{\mu_c^3}{\rho_c^3 \varepsilon}\right)^{1/4} < d_{\max} < 0.1D \quad (33)$$

Finally, the mean droplet size can be interpreted as the Sauter mean diameter ( $d_{32}$ ) or the droplet size describing 50% of the cumulative volume droplet size distribution ( $d_{50}$ ). In general, both parameters are similar in liquid-liquid dispersions in pipes and can be estimated as a fraction of the maximum droplet size as found elsewhere (Angeli and Hewitt, 2000a; Karabelas, 1978; Paolinelli et al., 2018):

$$\bar{d} \cong 0.5d_{\max} \quad (34)$$

### 2.4. Estimation of the phase inversion point

The estimation of the phase inversion point of the liquid-liquid system is a sensitive part of the present model. Unfortunately, the inversion point of a liquid-liquid mixture does not only depend on the fluids physical properties (e.g., densities and viscosities) but also on the chemical composition of both liquids, the power dissipated in the mixture, and the wettability of the pipe surface (favoring one phase or the other) (Arashmid and Jeffreys, 1980; Brauner and Ullmann, 2002; Ioannou et al., 2005; Selker and Sleicher Jr., 1965). Moreover, the inversion phenomena can be given within an ambivalent region of phase concentrations as mentioned in Section 2.1. In systems that are not contaminated with surfactants, the inversion point can be approximated using the mechanistic model proposed by Brauner and Ullmann (2002) for hydrocarbon and water turbulent flow, which assumes that, at the inversion point, the surface energies of both configurations (water completely entrained into oil and *vice versa*) are the same:

$$\varepsilon_w^l = \frac{1}{1 + \tilde{\rho}^{0.6} \tilde{\mu}^{0.4}} \quad (35)$$

where  $\varepsilon_w^l$  is the volumetric fraction of water at which phase inversion will occur,  $\tilde{\rho} = \rho_o / \rho_w$  and  $\tilde{\mu} = \mu_o / \mu_w$  are the ratios of the densities and viscosities, respectively, for the oil (indicated as subscript "o") and water (indicated as subscript "w") phases. It is worth mentioning that Eq. (35) neglects the effect of pipe surface wettability,

which may be important in small pipe diameters with very favorable wettability to either one or the other phase.

Unfortunately, Eq. (35) does not apply for contaminated systems where the inversion point or inversion region is affected by the influence of surface active compounds. These surfactants can reduce the interfacial tension and/or form interfacial films that alter significantly the dispersed phase volume fractions where phase inversion takes place and produce considerable hysteresis and ambivalence as discussed elsewhere (Brauner and Ullmann, 2002). For example, mixtures of water or brines in crude oils, which naturally contain organic acids, waxes, resins and asphaltenes, usually show inversion points around 50% water volume fraction or more independently of the oil densities and viscosities (Plasencia et al., 2013). These values are significantly larger than predicted by Eq. (35) or other empirical correlations based on mineral oils such as (Arirachakaran et al., 1989). Given the complexity of contaminated systems, it is evident that in such cases the inversion point needs to be determined experimentally. Benchtop tests in stirred vessels using small fluid quantities can be an alternative.

### 3. Model results and discussion

#### 3.1. Distribution of dispersed phase across the pipe section

In this section, the sub-model employed to calculate the local distribution of dispersed phase at the pipe cross-section (Eq. (13) and its closed-form solution (23)) is compared with experimental data available in the literature and obtained using traversing gamma densitometry in oil-water horizontal pipe flow (Elseth, 2001; Kroes et al., 2013; Valle, 2000). The properties of the used fluids and the characteristics of the experimental facilities are listed in Table 1. The selected experimental data accounts for cases of fully dispersed flow, where both water and oil droplet concentrations across the pipe section ( $C_w$  and  $C_o$ , respectively) are about 50% or lower, and it is assumed that one phase is completely entrained into the other. The mean water volumetric fraction in the flows is referred to as water cut (WC).

Figs. 1 and 2 show experimental and modeled volumetric fractions of dispersed phase droplets across the vertical pipe axis for different mixture velocities and water cuts in water-in-oil and oil-in-water horizontal flows, respectively. In general, the model agrees well with the experimental data. This is encouraging since Eq. (13) adopts several simplifications; for example, a single mean droplet size to represent the entire droplet population; a simple homogenous model to calculate the friction produced by the flow and the dissipated power (Eqs. (18) and (29), respectively), as well as the other assumptions mentioned above. Some over prediction of droplet accumulation at dispersed phase fractions larger than 20% and mixture velocities above 2 m/s are observed in some cases (e.g., left-middle and bottom-right graphs in Fig. 1 and right-top and right-bottom graphs in Fig. 2). This might be mainly related to one or a combination of factors such as under prediction of the flow friction and/or over prediction of the actual droplet sizes at high dispersed phase volume fractions, as discussed in the following sections. It is noteworthy that, in some cases, the measured dispersed phase concentrations at the locations of major accumulation (bottom and top of the pipe for dispersed water and oil, respectively) can be significantly different very close to the pipe wall. The presence of near-wall hydrodynamic forces (e.g., Saffman type (Saffman, 1965)), which usually tend to push droplets towards the pipe core, might explain the lower droplet concentrations measured close to the pipe wall. On the other hand, the existence of segregated thin films or rivulets of the dispersed phase flowing on the pipe wall, which leads to an apparent increase of the local dispersed phase concentration (Paolinelli et al., 2018),

might be the reason for the larger measured droplet concentrations. However, some of the effects seen close to the pipe walls could also be related to experimental artifacts.

Regardless of the discrepancies seen in some of the comparisons between the experimental data and the modeled droplet concentrations very close to the pipe wall ( $y/D < 0.05$  and/or  $y/D > 0.95$ ), the model can predict reasonably well accumulation of dispersed droplets across the pipe height with an average absolute relative error of 19% within the data range  $0.05 \leq y/D \leq 0.95$ .

#### 3.2. Prediction of dispersed flow pattern transition

In this section, the proposed model to predict dispersed flow pattern transition is compared with several sets of experimental data of flow patterns of mineral oil and crude oil and water flow in pipes. There are numerous experimental studies covering these fluids characteristics published in the literature. However, only some of these studies fulfil certain requisites that are crucial when comparing to theoretical models:

- Use of adequate techniques to properly detect the occurrence of dispersed flow regimes with oil or water as a full continuous phase across the pipe section. For example, the use of electrical probes (e.g., conductance and/or impedance) (Angeli and Hewitt, 2000b; Flores, 1997; Lovick and Angeli, 2004; Nädler and Mewes, 1997; Trallero, 1995; Zhai et al., 2015), and gamma densitometry has been very useful to detect full continuous flow regimes (Amundsen, 2011; Elseth, 2001; Kroes et al., 2013; Valle, 2000). In general, visual observation (e.g., clear section with high speed camera) has been the most employed method for characterizing flow regimes. However, accurate determination of full continuous flow regimes using only this technique can be difficult and ambiguous as discussed elsewhere (Amundsen, 2011; Angeli and Hewitt, 2000b; Nädler and Mewes, 1997). Therefore, experimental flow pattern maps that are only based on visual observation are not preferable due to their larger degree of uncertainty compared to the ones aided by other phase detection techniques, especially when describing the transition between dispersed to segregated flows.
- Use of a low shear mixer at the injection of the oil and water phases to allow for the intrinsic friction of the pipe flow to be the main source of turbulence. In addition, the pipe length ( $l$ ) must be long enough to allow flow to develop before reaching the assessment location of the flow rig. Full development of dispersed flows may take relatively large residence times due to the constant evolution of dispersed droplet sizes (Kostoglou and Karabelas, 2005). Pipe length is usually a limiting factor in lab facilities, where ratios of pipe length over pipe diameter between 150 and 400 have been usually used.
- Proper separation of the fluids after the circulation cycles.
- Use of wide ranges of mixture velocities and water cuts.
- Knowledge of all the physical properties of the fluids (e.g., density, viscosity and interfacial tension).

All the experimental studies considered in this work as well as the physical properties of the used fluids and details of the employed flow rigs are listed in Table 1.

The critical mixture velocity for the transition from dispersed to stratified flow is calculated for a given water cut ( $\varepsilon_w$ ) by solving iteratively Eq. (12) ( $C_{b,t} = IP$ ) simultaneously with Eq. (21) (droplet settling velocity). It must be noticed that when oil is the continuous phase ( $\varepsilon_w < \varepsilon_w^c$ ),  $IP = \varepsilon_w^c$ . On the other hand, when water is the continuous phase ( $\varepsilon_w > \varepsilon_w^c$ ),  $IP = 1 - \varepsilon_w^c$ .

**Table 1**  
Experimental oil-water flow studies considered for the model validation.

| Author                        | Fluids                                     | $\rho_o$<br>(kg/m <sup>3</sup> ) | $\rho_w$<br>(kg/m <sup>3</sup> ) | $\mu_o$<br>(mPa.s) | $\mu_w$<br>(mPa.s) | $\sigma$<br>(mN/m) | D (cm) | l/D  | Inclination | Pipe material   | Fluid injection/mixer                     | Flow pattern or phase distribution characterization method |
|-------------------------------|--|----------------------------------|----------------------------------|--------------------|--------------------|--------------------|--------|------|-------------|-----------------|---|--|
| Trallero (1995)               | Crystex AF-M, water                        | 884                              | 1037                             | 28.8               | 0.97               | 36                 | 5.01   | ~280 | Horizontal  | Acrylic         | Y junction, stratified entrance           | Visual observation and conductance probe                   |
| Nädler and Mewes (1997)       | Shell Ondina 17, water                     | 845                              | 997                              | 22–35              | 0.85               | —                  | 5.8    | ~225 | Horizontal  | Acrylic         | Cone-shaped junction, stratified entrance | Visual observation and conductance probe                   |
| Flores (1997)                 | Crystex AF-M, water                        | 850                              | 1000                             | 20                 | 1                  | 33.5               | 5.08   | ~300 | 45° to 90°  | Acrylic         | T junction                                | Visual observation and conductance probe                   |
| Alkaya et al. (2000)          | Crystex AF-M and Tusco 6016 mix, tap water | 849                              | 994                              | 12.9               | 0.72               | 36                 | 5.01   | ~300 | -2° to 2°   | Acrylic         | T junction                                | Visual observation and conductance probe                   |
| Angeli and Hewitt (2000b)     | Exxol D80, tap water                       | 801                              | 1000                             | 1.6                | 1                  | 17                 | 2.4    | ~370 | Horizontal  | Acrylic         | T junction                                | Visual observation and impedance probe                     |
| Valle (2000)                  | Oil 1 (crude oil and Exxol mix), water     | 755                              | 1000                             | 0.88               | 0.5                | 20                 | 5.63   | >300 | Horizontal  | Stainless steel | T junction                                | Gamma densitometry   |
|                               | Oil 2 (crude oil and Exxol mix), water     | 775                              |                                  | 1.1                |                    | 20                 |        |      |             |                 |   |  |
| Elseth (2001)                 | Exxol D60, tap water                       | 790                              | 1000                             | 1.64               | 1                  | 43                 | 5.63   | ~180 | Horizontal  | Stainless steel | Y junction, stratified entrance           | Visual observation and gamma densitometry                  |
| Lovick and Angeli (2004)      | Exxol D140, tap water                      | 828                              | 1000                             | 6                  | 1                  | 39.6               | 3.8    | ~210 | Horizontal  | Stainless steel | T junction                                | Visual observation, conductance and impedance probe        |
| Rodriguez and Oliemans (2006) | Shell Vitrea 10, water                     | 831                              | 1070                             | 7.17               | 0.76               | 36                 | 8.28   | ~180 | -5° to 5°   | Stainless steel | T junction                                | Visual observation   |
| Vielma et al. (2008)          | Tulco Tech 80, tap water                   | 858                              | 1000                             | 18.8               | 1                  | 28.5               | 5      | ~270 | Horizontal  | Acrylic         | Y stratified entrance                     | Visual observation and conductance probe                   |
| Kumara et al. (2009)          | Exxsol D60, water                          | 790                              | 996                              | 1.64               | 1                  | 43                 | 5.6    | ~270 | -5° to 5°   | Stainless steel | Y stratified entrance                     | Visual observation and gamma densitometry                  |
| Kroes et al. (2013)           | Crude oil A                                | 850                              | 1000                             | 6.2                | 0.89               | 16                 | 5.2    | ~300 | Horizontal  | Stainless steel | Y stratified entrance                     | Gamma densitometry   |
|                               | Crude oil B-LS                             | 810                              | 1000                             | 3.2                | 1                  | 16                 |        |      |             |                 |   |  |
|                               | Crude oil B-HS                             |                                  | 1150                             |                    | 1.4                | 16                 |        |      |             |                 |   |  |
| Zhai et al. (2015)            | Mineral oil, water                         | 845                              | 1000                             | 12                 | 1                  | 35                 | 2      | ~150 | Horizontal  | Acrylic         | T junction                                | Visual observation and conductance probes                  |

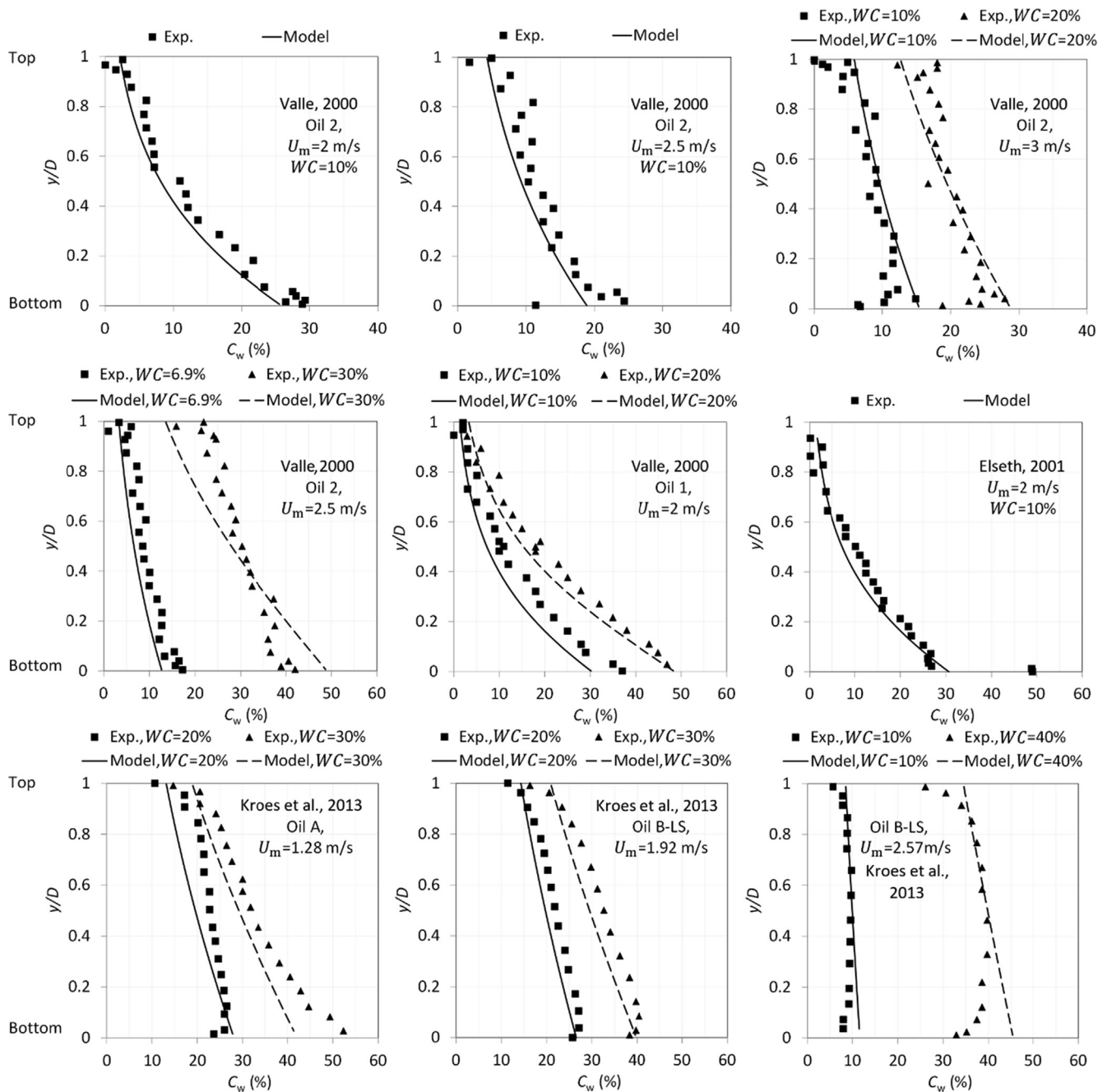


Fig. 1. Experimental and modeled distribution of dispersed water volumetric fraction across the pipe vertical axis in dispersed water-in-oil horizontal flow.

### 3.2.1. Horizontal flow

The sets of experimental data that are assessed at the first part of this section (Figs. 3–12) were produced using clear mineral oils and water as fluids. These systems can be considered as non-contaminated or slightly contaminated; and thus, their phase inversion point can be fairly estimated from mechanistic models such as Eq. (35) in case it is not measured.

Figs. 3–9 show the experimental flow pattern maps by Trallero (1995), Nädler and Mewes (1997), Alkaya et al. (2000), Angeli and Hewitt (2000b), Lovick and Angeli (2004), Vielma et al. (2008), and Zhai et al. (2015), respectively, along with the stability bounds for dispersed flow modeled using the criterion  $C_{b,t} = IP$  (Eq. (12)), as well as the commonly employed criteria in Eqs. (9) and (10) referred to as Brauner's model. These flow maps were obtained by visual observation and conductance or impedance probes to

help determine full continuous phase flow patterns. For the sake of simplicity, the original flow pattern nomenclature made by some of the authors (Angeli and Hewitt, 2000b; Elseth, 2001; Lovick and Angeli, 2004; Nädler and Mewes, 1997) was changed to match the classifications mentioned in the introduction section. The phase inversion point of the systems in Figs. 3, 5, 8 and 9 were calculated using Eq. (35) (water volume fractions of 22%, 26%, 25% and 29%, respectively) since the authors did not report any certain evidence on the phase volume fraction in which inversion might have occurred. Nadler and Mewes (Fig. 4) reported that phase inversion was given for water volume fractions between 10% and 20% from analyzing their pressure drop results. The latter value, which is close to the value of 22% calculated by (35), was used in the present model. Angeli and Hewitt tested flows in acrylic (Fig. 6a) and stainless steel (Fig. 6b) pipes. They inferred that phase

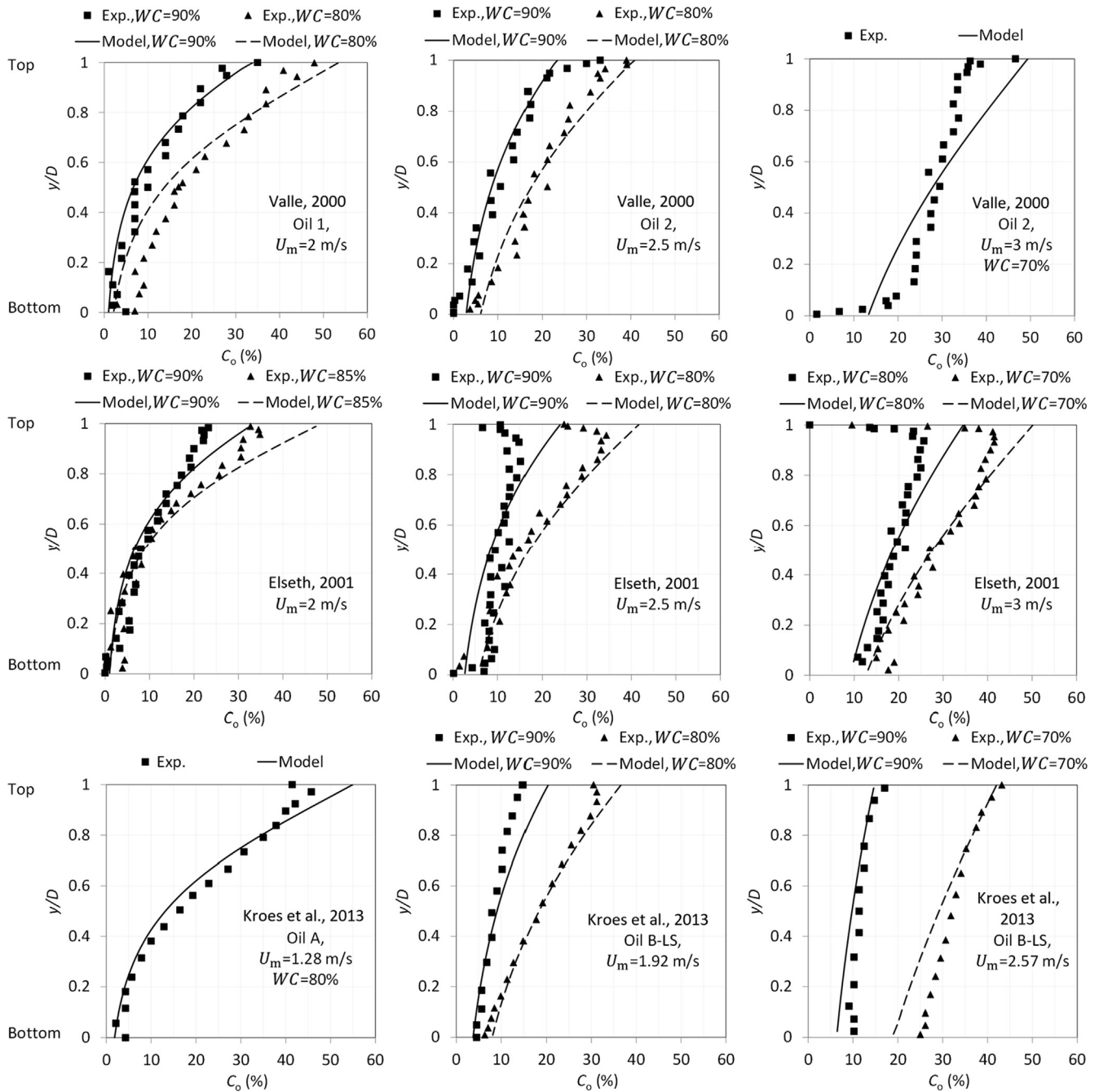


Fig. 2. Experimental and modeled distribution of dispersed oil volumetric fraction across the pipe vertical axis in dispersed oil-in-water horizontal flow.

inversion occurred at around 37–40% input water volume fraction for both pipes from their pressure drop data (Angeli and Hewitt, 1999). An average value of 38.5% water volume fraction was used for the current model assessment. In addition, the reported wall roughness of  $1 \times 10^{-5}$  m (~hydraulically smooth pipe) and  $7 \times 10^{-5}$  m were used for the calculation of the friction of the acrylic and the stainless steel pipes, respectively. Lovick and Angeli (Fig. 7) reported that phase inversion took place at 32% water input fraction from their results in pipe flow at high mixture velocities and additional work in a stirred vessel.

From Figs. 3 to 9, it can be seen that the criterion  $C_{b,r} = IP$  (black solid lines) agrees very well with the experimental transitions from oil continuous regimes (D W/O and D W/O & O) and water continuous regimes (D O/W and D O/W & W) to segregated regimes (e.g.,

ST & MI, D O/W & W/O, D W/O & W). It is worth noting that the proposed model corresponds well the experimental trend on the slope of transition from continuous to segregated regimes, which becomes very steep in terms of the increment of critical mixture velocities when dispersed phase volume fractions get close to the inversion point; for example, as indicated by the transitions measured by Angeli and Hewitt shown by the black short-dash lines in Fig. 6.

Fig. 10 shows the experimental flow pattern map obtained by Elseth (2001) only using visual observation (Fig. 10a), as well as another flow pattern map using Elseth's gamma densitometry data (Fig. 10b) reclassified by Kroes et al. (2013) Kroes et al. assumed that the inversion point of Elseth's oil-water system occurred at a water volume fraction of 50%, which is similar to the value of

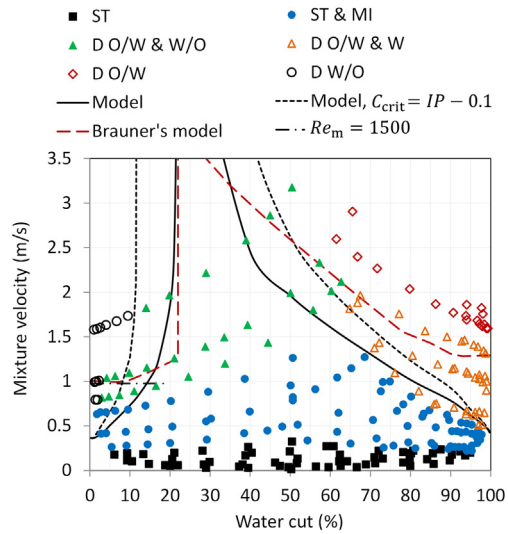


Fig. 3. Experimental flow pattern map from Trallero (1995). Comparison with the proposed model and Brauner's model.

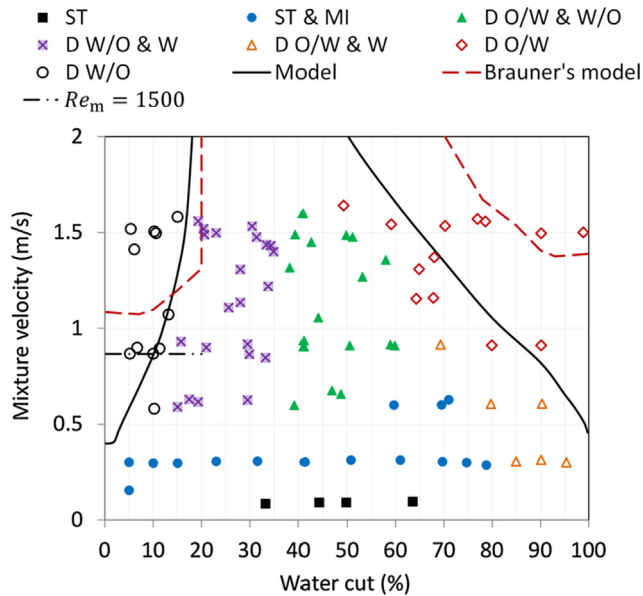


Fig. 4. Experimental flow pattern map from Nädler and Mewes (1997). Comparison with the proposed model and Brauner's model.

49% calculated by (35) and used in the model. Comparing both maps, it is clear that the visual interpretation of oil continuous and water continuous dispersed flows originally made by Elseth; e.g.: D W/O, D W/O & O, D O/W & W, D O/W H (homogeneous) and D O/W I (inhomogeneous), do not correlate well with his gamma densitometry data which captured more reliably the occurrence of phase segregation. In this case, visual observation favored the notion that oil and water continuous regimes still occurred at lower mixture velocities and higher dispersed water fractions, while segregation was actually taking place. It is worth noting that the proposed model matches very well the experimental transition from dispersed to separated flows measured with gamma densitometry (Fig. 10 b).

The experimental data shown in Rodriguez and Oliemans (2006) (Fig. 11) that corresponds to flows with relatively large diameter (0.083 m) as well as Kumara et al. (2009) (Fig. 12) that covers operating conditions at very low dispersed phase fractions

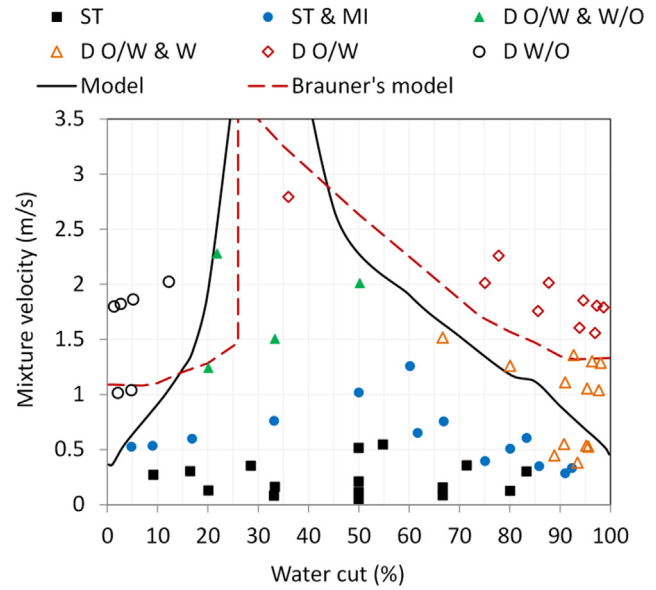


Fig. 5. Experimental flow pattern map from Alkaya et al. (2000). Comparison with the proposed model and Brauner's model.

are also included in the model validation, despite that both flow pattern maps were determined by visual observation only. The inversion point of the systems shown in Figs. 11 and 12 were estimated using (35) as 32% and 49% water volume fractions, respectively. The modeled transition lines coincide well with the experimental transition between oil or water continuous and separated flows. In the case of the flow pattern map by Kumara et al., the model seems to over predict critical mixture velocities with respect to the experimental transition from water continuous with inhomogeneous oil distribution (D O/W & W) to separated mixed flows (e.g., D O/W & W/O), although it reproduces well the slope of this transition and shows an excellent fit with the transition from water continuous with homogeneous oil distribution (D O/W) to D O/W & W regimes.

Fig. 13 show flow pattern maps of crude oil and water flows by Kroes et al. (2013) determined from gamma densitometry results. The authors inferred the inversion point of all the shown systems was about 50% water volume fraction from their pressure drop recordings. The same value was used as an input of the present model. The predicted transition bounds agree very well with the experimental transition from dispersed to stratified flows.

### 3.2.2. Inclined flow

The criterion used in the present model for dispersed flow stability (Eq. (12)) can also be applied to inclined flows. Buoyancy or gravity effects on droplet sedimentation towards the pipe wall decreases when the pipe is inclined upwards or downwards, due to the contribution of only a portion of the volume force on dispersed droplets (vertical component with respect to the pipe axis). This effect is taken into account in the model by using the vertical component of the droplet settling velocity ( $U_{s,y}$ , Eq. (14)) in the transport Eq. (13). Pipe inclination can cause slip between phases even in fully dispersed flows due to the volume forces acting in the main flow direction (Flores, 1997; Mukherjee et al., 1981). Moreover, as result of these volume forces, complex flow features such as counter current separated flows, pseudo slug or plug flow, and counter current motion of dispersed droplets and/or globules can be present (Flores, 1997; Lum et al., 2006; Vigneaux et al., 1988; Zavareh et al., 1988), especially at pipe inclinations larger than  $10^\circ$ . As mentioned in previous sections, slip between phases is neglected in the current modeling.

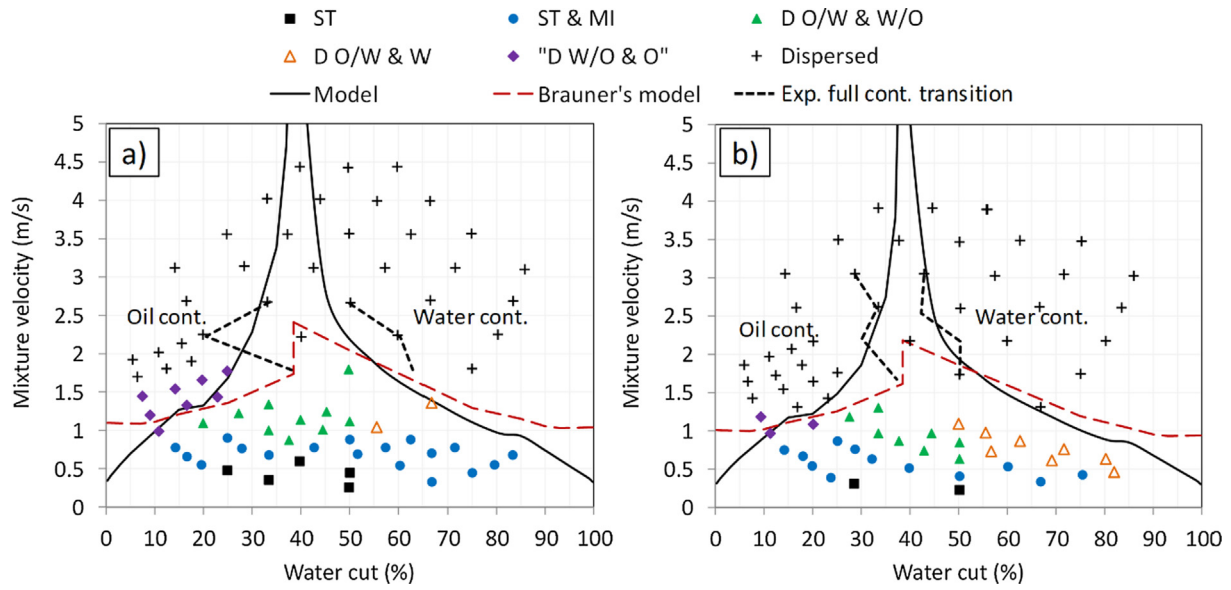


Fig. 6. Experimental flow pattern map from Angeli and Hewitt (2000b): (a) Acrylic pipe, (b) stainless steel pipe. Comparison with the proposed model and Brauner's model.

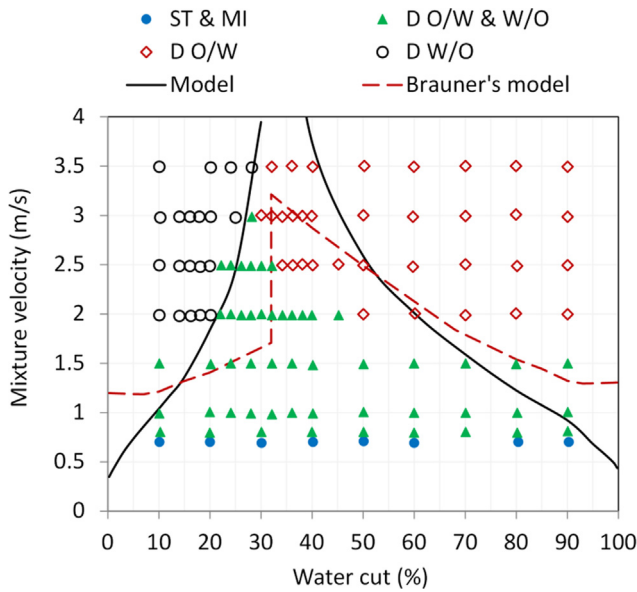


Fig. 7. Experimental flow pattern map from Lovick and Angeli (2004). Comparison with the proposed model and Brauner's model.

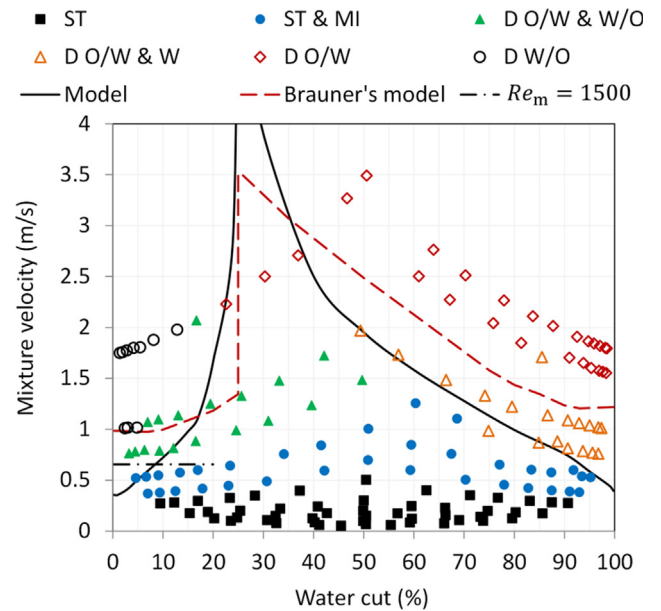


Fig. 8. Experimental flow pattern map from Vielma et al. (2008). Comparison with the proposed model and Brauner's model.

Fig. 14 shows flow pattern maps of mineral oil and water with significant upward inclinations of 45°, 60° and 75° obtained by Flores (1997) using visual observation and conductance probes. The inversion point of the used system was calculated using (35) as 25% water volume fraction. It is worth mentioning that when fully dispersed regimes are no longer stable in these inclined flows, complex flow patterns are found such as “transitional flow” (TF, separated oil and water layers with dispersed droplets of each phase and a mixed interface), “dispersion of oil in water counter-current” (D O/W CT, oil flows as dispersed droplets segregated at the pipe top and the water layer presents countercurrent flow at the pipe bottom), and “dispersion of oil in water pseudo slugs” (D O/W PS, oil flows as dispersed droplets and globules segregated at the pipe top that form dense packs separated alternatively by water, recirculation of oil droplets is given due to water counter-current flow at the pipe bottom). At higher mixture velocities oil

is well dispersed in water as is the case of “dispersion in oil water co-current” (D O/W CC, oil flows dispersed mainly occupying the upper half of the pipe, no counter current flow of water occurs) and “very fine dispersion of oil in water” (VFD O/W, oil droplets are homogeneously dispersed across the pipe section). Water in oil dispersions are named D W/O and “very fine dispersion of water in oil” (VFD W/O, water droplets are homogeneously dispersed across the pipe section). The present model represents well the transition from oil continuous regimes (D W/O and VFD W/O) to separated and water continuous regimes for 45° and 60° inclinations. However, for 75° inclination, it overpredicts the critical mixture velocities for water fractions above 20% where the separated “transitional flow” regime was only observed at mixture velocities around 0.5 m/s or lower. The model also predicts well the transition between water continuous co-current regime

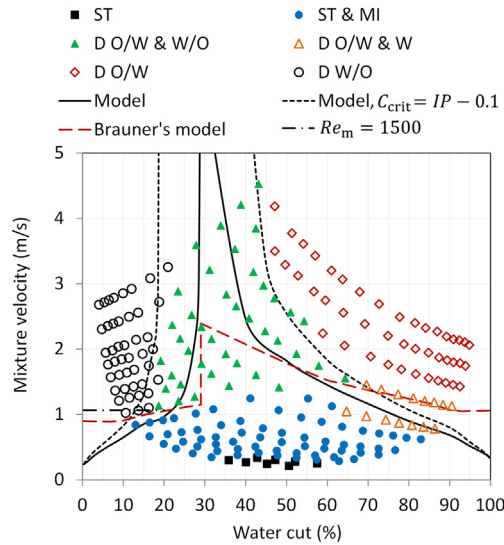


Fig. 9. Experimental flow pattern map from Zhai et al. (2015). Comparison with the proposed model and Brauner's model.

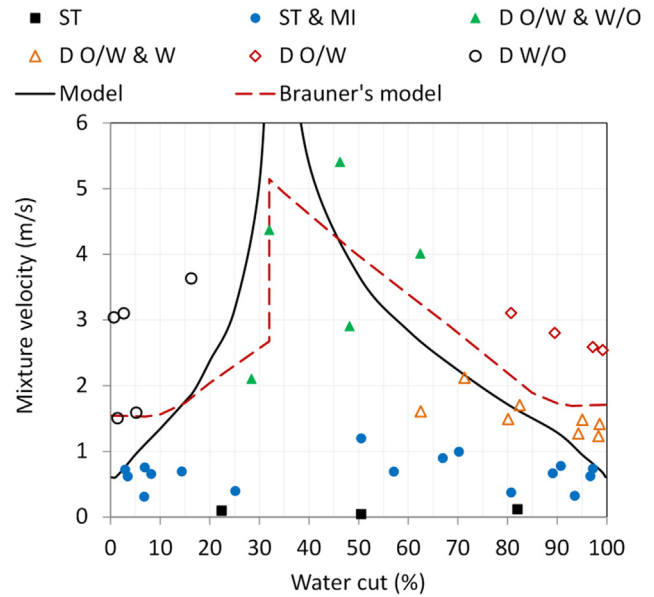


Fig. 11. Experimental flow pattern map from Rodriguez and Oliemans (2006). Comparison with the proposed model and Brauner's model.

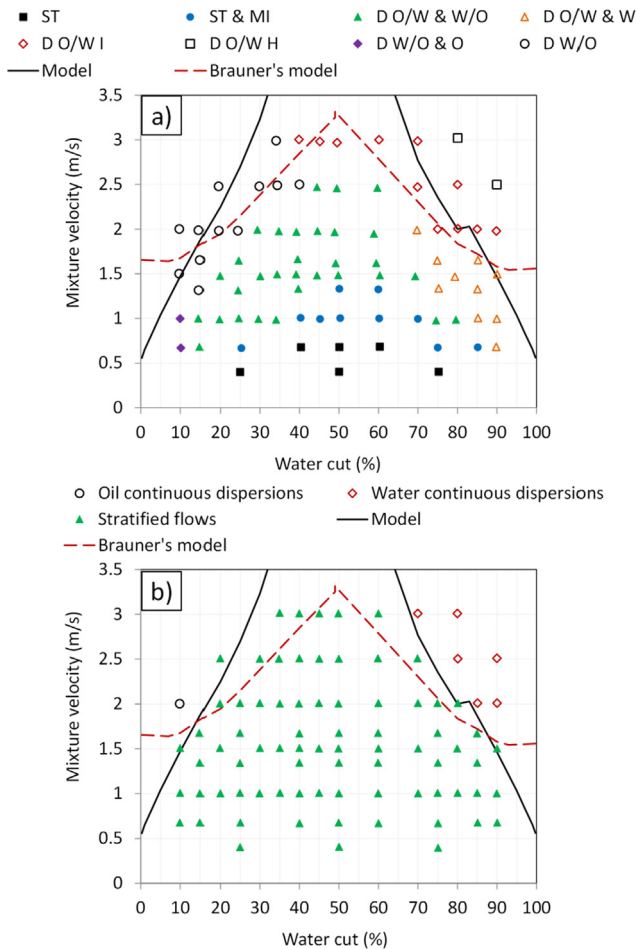


Fig. 10. Experimental flow pattern maps from: (a) Elseth (2001), and (b) Kroes et al. (2013). Comparison with the proposed model and Brauner's model.

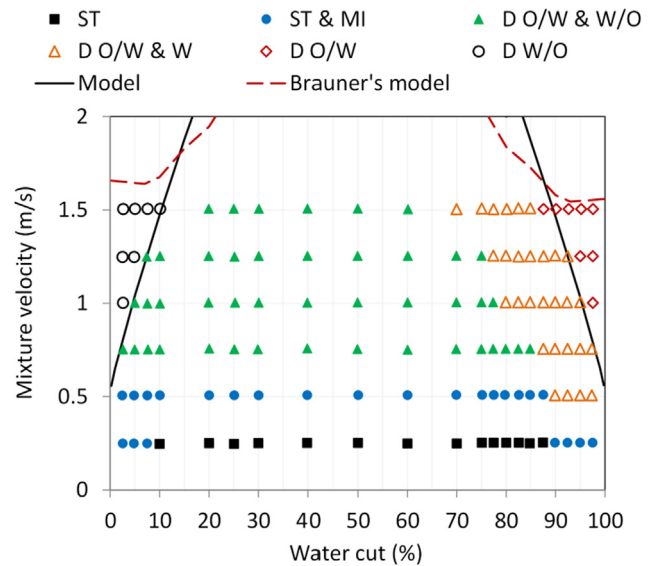


Fig. 12. Experimental flow pattern map from Kumara et al. (2009). Comparison with the proposed model and Brauner's model.

dispersed oil in water regimes in which the continuous phase is assumed to flow in the pipe direction with no or negligible net cross flow. From this point of view, the model works very well describing the transition from dispersed co-current to counter current flows. The over prediction of the critical mixture velocities for D O/W CC regime for water contents lower than 70% and larger than the inversion point may be partly related to the significant slip between the dispersed oil and continuous water phases as reported by Flores (1997), which reduced the oil holdup as much as 20% for co-current flows and 60% for counter current flows.

### 3.2.3. Comparison of the model with other commonly used criteria

When comparing the model predictions with the generally used criteria of Eqs. (9) and (10) suggested by Brauner (2001) and the experimental data, it is evident that the introduced criteria of

(D O/W CC) and pseudo slug and counter current regimes (D O/W PS and D O/W CT) for water volume fractions larger than 70%. It is worth bearing in mind that both of these latter two regimes showed counter currents and cannot be considered as regular fully

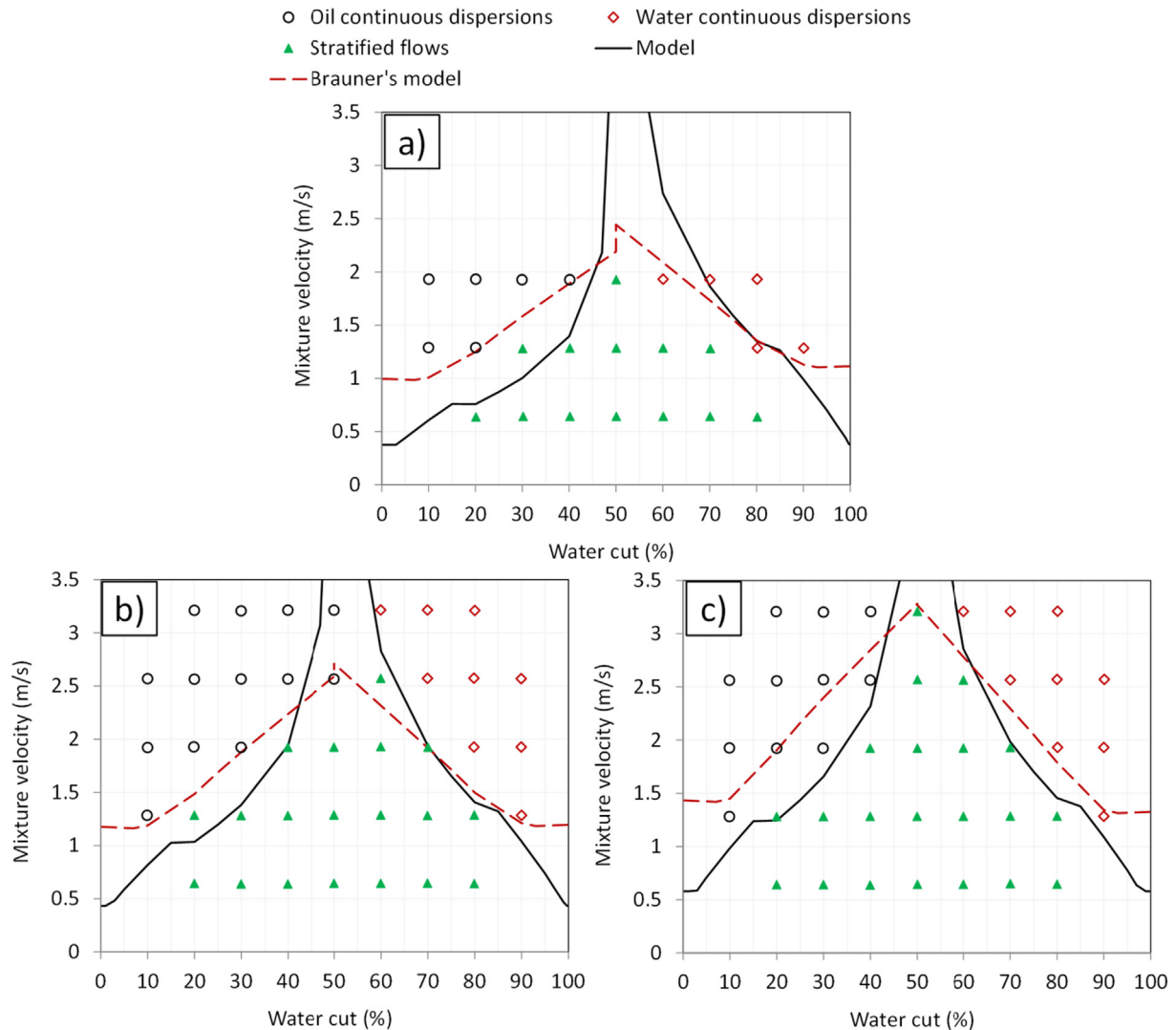


**Fig. 13.** Experimental flow pattern maps from Kroes et al. (2013): (a) crude oil A, (b) crude oil B-LS, and (c) crude oil B-HS. Comparison with the proposed model and Brauner's model.

critical droplet concentration (Eqs. (11) and (12)) describes better the stability bounds of dispersed flows in the entire range of phase volume fractions. As already mentioned above, the model follows very well the slope of the experimental transition from dispersed to segregated flows seen in the numerous systems with different fluids, pipe diameters and inclinations shown in Figs. 3–14. These experimental slopes tend to be quite abrupt when dispersed phase volume fractions are close to the inversion point, which is well captured by the model where critical mixture velocities increase and tend to be infinite as volume fraction of dispersed phase gets very close to the selected critical concentration. Contrarily, this behavior is not addressed by Brauner's criteria (red dashed lines in Figs. 3–14) in which the increase of critical mixture velocities with dispersed phase volume fraction is only given by the growth of dispersed droplet sizes (Eq. (30)), overlooking the actual concentration of dispersed phase at the bottom or top of the pipe. For example, this can lead to important under prediction of critical mixture velocities for dispersed phase volume fractions close to the inversion point, especially when phase inversion occurs at volume fractions significantly lower than 50% (see Figs. 3, 5 and 6–9).

One of the main advantages of the present model compared to any of the available criteria mentioned in the introduction section

is that it predicts the stability of dispersed flow based not only on the properties of the fluids and pipe geometry but also on the inversion point of the liquid-liquid system. This is extremely important when assessing crude oil systems or any other system that is considered as “contaminated” and its inversion point takes place at considerably larger water volume fractions than predicted for “non-contaminated” systems using mechanistic models such as (35); especially, when the oil viscosity is significantly larger than the water viscosity. Fig. 15 shows a hypothetical example of dispersed flow bounds predicted by the introduced model (criterion  $C_{b,t} \leq IP$ ) and the classic criteria  $d_{max} \leq d_{crit}$  for a given oil-water system where the phase inversion point is calculated by Eq. (35) as  $\sim 35\%$  water volume fraction, but if contaminated with surfactants it increases to 50% water volume fraction as commonly seen for crude oils. According to the proposed model, the shift of the inversion point from 35% to 50% water volume fraction basically decreases the critical mixture velocities for dispersion of water in oil and increases critical mixture velocities for dispersion of oil in water. Both effects are quite significant when the volume fractions of dispersed phase are higher than 10%. This behavior is also seen in the experiments; for example, when comparing the flow map of a “non-contaminated” mineral oil system such as the one of Lovick

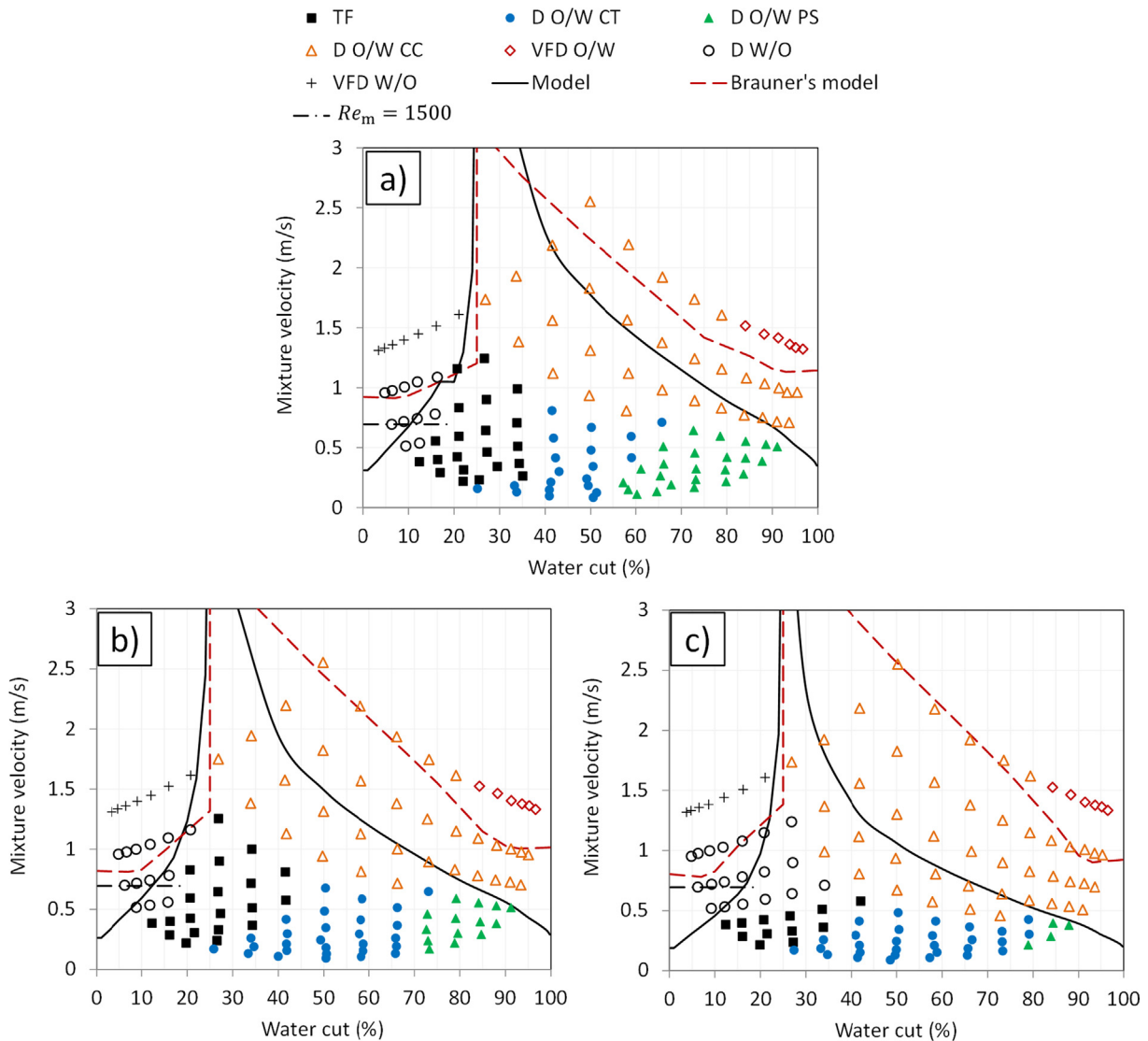


**Fig. 14.** Experimental flow pattern maps from Flores (1997): (a) 45° upward flow, (b) 60° upward flow, and (c) 75° upward flow. Comparison with the proposed model and Brauner's model.

and Angeli ( $\tilde{\rho} = 0.83$ ,  $\tilde{\mu} = 6$ ,  $\sigma = 40 \text{ mN/m}$ ,  $IP = 32\%$ ,  $D = 0.038 \text{ m}$ , Fig. 7) with the crude oil system of Kroes et al. ( $\tilde{\rho} = 0.85$ ,  $\tilde{\mu} = 6.2$ ,  $\sigma = 16 \text{ mN/m}$ ,  $IP = 50\%$ ,  $D = 0.05 \text{ m}$ , Fig. 13a). Despite the differences in the interfacial tension and the pipe diameter of these systems, the inversion point of both systems should be around 35% water volume fraction (Eq. (35)), which is true for the mineral oil system but not for the crude oil. This leads to important differences such as that the mineral oil system does not fully disperse water in oil, for water cuts between 25% and 30%, until reaching mixture flow velocities larger than 3 m/s, which is very well predicted by the present model but severely underpredicted by Brauner's criteria. On the other hand, the crude oil system is fully dispersed at the same water cuts at mixture velocities above 1.5 m/s, which again is well predicted by the present model; and also in this case, by the classic criteria that shows very similar transition lines for both the mineral oil and the crude oil systems when in fact the experimental behavior is quite different. Additionally, Brauner's criteria tend to over predict critical mixture velocities for dispersed flow when dispersed phase volume fractions are lower than 10% as seen from the flow maps in Figs. 3–5, 8, 12 and 14, while the introduced model performs better. This is a critical feature for industrial

applications such as horizontal lines for crude oil and product transportation in which water exist as contaminant in low volume fractions (e.g., <5%) and, it is of extreme importance to know without much conservatism whether segregation will occur or not to avoid possible corrosion problems.

Concerning the effect of pipe diameter on the critical mixture velocities for dispersed flow, the present model predicts an increase of critical mixture velocities with pipe diameter as shown in Fig. 16 for hypothetical cases of pipe diameters of 0.05 m, 0.15 m and 0.3 m. This is a trend that the classic criteria suggested by Brauner also predict (red thick lines in Fig. 16). It is worth mentioning that the use of the current model may have limitations for flows in very small pipe diameters as discussed in a further section.

### 3.3. Possible model refinements

#### 3.3.1. Setting of critical droplet concentration

As mentioned above, significant coalescence of dispersed phase droplets and consequent phase segregation can occur at droplet concentrations lower than the inversion point. Moreover, phase inversion phenomenon usually takes place in a range of phase vol-

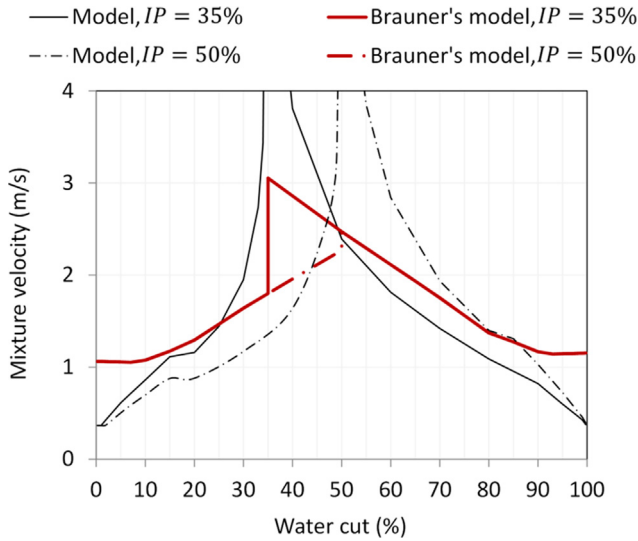


**Fig. 15.** Comparison of modeled transition bounds for dispersed flow for different phase inversion points ( $IP$ ).  $\rho_o = 850 \text{ kg/m}^3$ ,  $\rho_w = 1000 \text{ kg/m}^3$ ,  $\mu_o = 5 \text{ mPa}\cdot\text{s}$ ,  $\mu_w = 1 \text{ mPa}\cdot\text{s}$ ,  $\sigma = 20 \text{ mN/m}$ ,  $D = 0.05 \text{ m}$ ,  $\beta = 0^\circ$ .

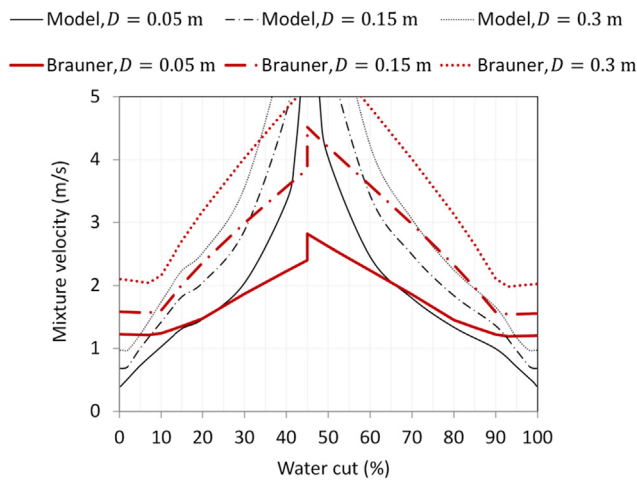


**Fig. 16.** Comparison of modeled transition bounds for dispersed flow for different pipe diameters.  $\rho_o = 830 \text{ kg/m}^3$ ,  $\rho_w = 1000 \text{ kg/m}^3$ ,  $\mu_o = 2 \text{ mPa}\cdot\text{s}$ ,  $\mu_w = 1 \text{ mPa}\cdot\text{s}$ ,  $\sigma = 20 \text{ mN/m}$ ,  $IP = 45\%$ ,  $\beta = 0^\circ$ .

ume fractions instead of a single value. Therefore, setting the critical droplet concentration at; for example, 10% of volume fraction less than the inversion point (based on the dispersed phase volume) can lead, in some cases, to better prediction of the transition bounds from dispersed to stratified flow as shown black short-dash lines in Figs. 3 and 9.

### 3.3.2. Enhancement of the used sub-models

Several sub-models are used to evaluate the criterion  $C_{b,t} \leq IP$  as shown in previous sections. Some of these models can be enhanced to obtain better predictions at the price of adding more complexity for their implementation:

- **Calculation of dispersed droplet sizes:** The calculation of droplet sizes can also be performed using population balance methods (Kostoglou and Karabelas, 2005), which are more comprehensive than the equations shown in Section 2.3 and can account for the effect of residence time on the size of flowing droplets. However, the implementation of such an approach greatly increases complexity for practical

purposes. It is worth mentioning that the effect of dispersed phase viscosity on droplet sizes is neglected in the model. Thus, if relatively high dispersed phase viscosities (e.g.,  $>100 \text{ mPa}$ ) are to be assessed, it is recommended to use formulations that account for the internal viscous resistance of droplets against turbulent break-up (Hinze, 1955; Wang and Calabrese, 1986) to avoid excessive under prediction of droplet size. As stated in Section 2.3, droplet sizes are assumed to grow with the volume fraction of the dispersed phase (Eq. (31)), as also proposed in Brauner's model (Eq. (30) (Brauner, 2001)). This may not be true for some systems as reported elsewhere (Lovick et al., 2005; Simmons and Azzopardi, 2001). Thus, the use of more comprehensive formulation on this respect can definitely lead to better results.

- **Calculation of the flow friction:** Important parameters of the model such as the power dissipated by the flow (Eq. (29), which controls droplet sizes) and the friction velocity (Eq. (5), which controls droplet turbulent diffusion) are proportional to the friction between the mixed flow and the pipe wall represented by the friction factor in Eq. (18). As mentioned in Section 2.2, in some cases, the friction and pressure gradient of dispersed flows with dispersed phase volume fractions larger than about 20% and/or close to the inversion point can increase significantly with respect to the dilute dispersion behavior. This phenomenon is certainly complex and has been usually explained by the increase of the viscosity of the liquid-liquid mixture, which can be approximately described by the simple Brinkman's equation (Brinkman, 1952). This equation can be incorporated to the model for better predictions if needed.

- **Calculation of accumulation of dispersed droplets:** The use of more complex version of the transport Eq. (13) that accounts for multiple droplet sizes instead of a single mean droplet size to represent the entire droplet population (Karabelas, 1977) can help obtain better prediction of droplet accumulation as stated by Segev (1984). It is worth reminding that Eq. (13) does not consider near wall forces that may act on dispersed droplets due to the velocity gradient of the continuous phase boundary layer flow. Moreover, turbulent droplet diffusivity, which in the present model is considered to be constant across the pipe section, can differ from a location near pipe wall to the pipe core (Kaushal et al., 2002). To properly evaluate these effects that may or not be important with respect to the current given solution of Eq. (13), a two-dimensional advection-diffusion model must be used to solve the droplet concentration field across the entire pipe section involving a significant extra numerical effort (Segev, 1984). The addition of hindering correction terms such as Richardson and Zaki (1997) to account for the restriction of the flow of the continuous phase around dispersed droplets as dispersed phase volume increases should be also considered. These terms are not shown in the simplified steady state Eq. (13) since both settling and dispersive fluxes are affected the same way by hindering. However, hindering terms must be added when assessing transient behavior or when adding extra terms that are not believed to be significantly affected by hindering (e.g., Saffman type forces). Regarding droplet drag coefficients to calculate droplet sedimentation rates, low viscosity droplets moving in a larger viscosity continuous phase (e.g., water droplets in viscous oil) can experience internal recirculation currents that can reduce drag force as described by the correlations found elsewhere (Feng and Michaelides, 2001; Rivkind and Ryskin, 1976), leading

to higher settling velocities with respect to the use of the simpler Eq. (22). A key proviso is that the fluid-fluid interfaces are not significantly contaminated with surface active compounds that hamper their motion by partial or total coverage. Contaminated systems such as crude oils are prone to have altered interfaces with water making water droplets behave as solid-like in the oil flow; thus, Eq. (22) is still a good approximation. In case of inclined flow, a drift flux model can be further incorporated to account for the slip between phases and calculate the dispersed phase holdup more precisely, especially for oil in water flows and relatively high inclination angles (e.g.,  $\geq 45^\circ$ ) (Flores, 1997).

### 3.4. Model limitations

#### 3.4.1. Turbulent flow

The present model assumes that the mixed liquid-liquid flow is turbulent. As analogy to single phase flow, the Reynolds number of the mixed flow ( $Re_m$ ) should be around or larger than 2100 as proposed elsewhere (Brauner, 2001). However, some experimental data indicates that full dispersed flow can occur even at Reynolds numbers lower than 1500, as indicated with dash-dot lines in Figs. 3, 4 and 14. This is not surprising since the presence of dispersed droplets can distort stream lines, generate vorticity, and modify velocity gradients in the continuous phase favoring turbulent flow (Crowe, 2000). For example, some researchers have proposed limiting Reynolds numbers from 1000 to 1500 ((Sharma et al., 2011) and (Rodriguez and Oliemans, 2006), respectively) for their multiphase modeling. In view of the available experimental data, it is suggested to use a limiting Reynolds number of about 1500 for turbulent flow of the continuous phase and minimum mixture velocity for dispersed flow.

#### 3.4.2. Overlap with criteria for stratified flow stability

The introduced criterion for dispersed flow stability assumes that the mixed flow is already fully dispersed. However, the two liquids can also flow as fully stratified layers (which is the regime of lowest energy) if this configuration turns out to be stable. In general, the most adopted model to determine the stability of stratified flow regime is the stability analysis of interfacial waves performed based on the momentum equations of both liquid layers (Kelvin-Helmholtz instability (Brauner and Moalem Maron, 1992)). Although the analytical solution of these analyses is somewhat complex, a simplified assessment can be done by using the mixture Froude number ( $Fr_m$ ) with a value of 1.25 to determine the critical mixture velocity below which stratified flow can be stable (Al-Sarkhi et al., 2017):

$$Fr_m = \sqrt{\frac{\rho_o}{(\rho_w - \rho_o)gD \cos \beta}} U_m \quad (36)$$

where the subscripts "o" and "w" stand for oil and water, respectively.

In case the critical mixture velocity for dispersed flow calculated by (11) or (12) is lower than the critical mixture velocity for stability of stratified flow (from Eq. (36)), the latter should be adopted as the dispersed to segregated flow transition bound. This scenario can be plausible when assessing flows in relatively large pipe diameters (e.g.,  $>0.1$  m) and low dispersed phase volume fractions (e.g.,  $<5\%$ ).

#### 3.4.3. Pipe diameter and droplet size scale

The used criterion is implemented using a simplified steady state transport Eq. (13) that is well suited for fluids with relatively high viscosities and small density difference (as the case of oil and

water) since dispersed droplets attain their terminal settling velocity in very short distances ( $l_s$ ) that; in general, are  $<5\%$  of the pipe diameter. However, systems with relatively small diameter (e.g.,  $<0.02$  m) and high droplet settling velocities ( $U_s$ ) can lead to  $l_s/D$  ratios larger than 0.05. This may lead to important inaccuracy when estimating dispersed phase concentrations at the pipe cross-section using (13); thus, the following relation should be checked:

$$\frac{l_s}{D} \cong \frac{\rho_d U_s^2}{2|\rho_d - \rho_c|gD} < 0.05 \quad (37)$$

Regarding the size of dispersed phase droplets, it should not be larger than about 10% of the pipe diameter ( $d_{max} \leq 0.1D$ ). This is mainly due to the fact that the used close-form solution in Eq. (23) is based on the assumption that droplet sizes are very small compared to the diameter of the pipe. In general, these size scale limitations are not a problem in industrial turbulent liquid-liquid flows; for example, in the oil industry where internal pipe diameters are usually larger than 0.025 m and flow rates are considerably high.

#### 3.4.4. Calculation of droplet accumulation at very low dispersed phase volume fractions

The calculation of critical mixture velocities for dispersed flow regime via the concept of critical concentration (Eqs. (11) and (12)) may lead to some under prediction when the dispersed phase volume fractions are very low (e.g.,  $<1\%$ ), critical droplet concentration is relatively high (e.g.,  $>40\%$ ), and the pipe diameter is relatively small (e.g.,  $<0.02$  m). In these circumstances, very low mixture velocities would be required for the entire population of dispersed droplets to flow very close to the pipe wall and accumulate at critical concentrations; for example, occupying only about 1/5 of the pipe height according to Eq. (13). However, at low flow velocities, predicted equilibrium droplet sizes can actually be about a tenth of the pipe diameter, which is close to the size scale of the region where droplets are predicted to flow, and the assumptions discussed in Section 3.4.3 may not be met leading to unreliable results.

#### 3.4.5. Formation of emulsions

Some liquid-liquid systems can develop very tight emulsions due to the presence of surface active compounds that modify and stabilize the interfaces of dispersed droplets producing significant changes in the viscosity of the mixture, such as mentioned in Section 3.3.2, as well as rheological behavior (Pal, 1996) which greatly alters droplet sedimentation and dispersion respect to the assumptions made in the present model. In these cases, accumulation of dispersed phase droplets is expected to be significantly less than predicted by the model.

### 3.5. Model flow chart

Fig. 17 shows a flow chart of the model with a summary of its main decision structures and equations.

## 4. Summary and conclusions

A model to assess stability of dispersed turbulent liquid-liquid flow in horizontal and inclined pipes has been suggested. This model is more comprehensive of the physics of dispersed liquid-liquid flow than other criteria available in the literature to determine the transition from dispersed to segregated flows; e.g., as suggested by Brauner (2001). The model accounts for turbulent break-up of dispersed phase droplets, sedimentation and dispersion of droplets and their accumulation, and droplet coalescence

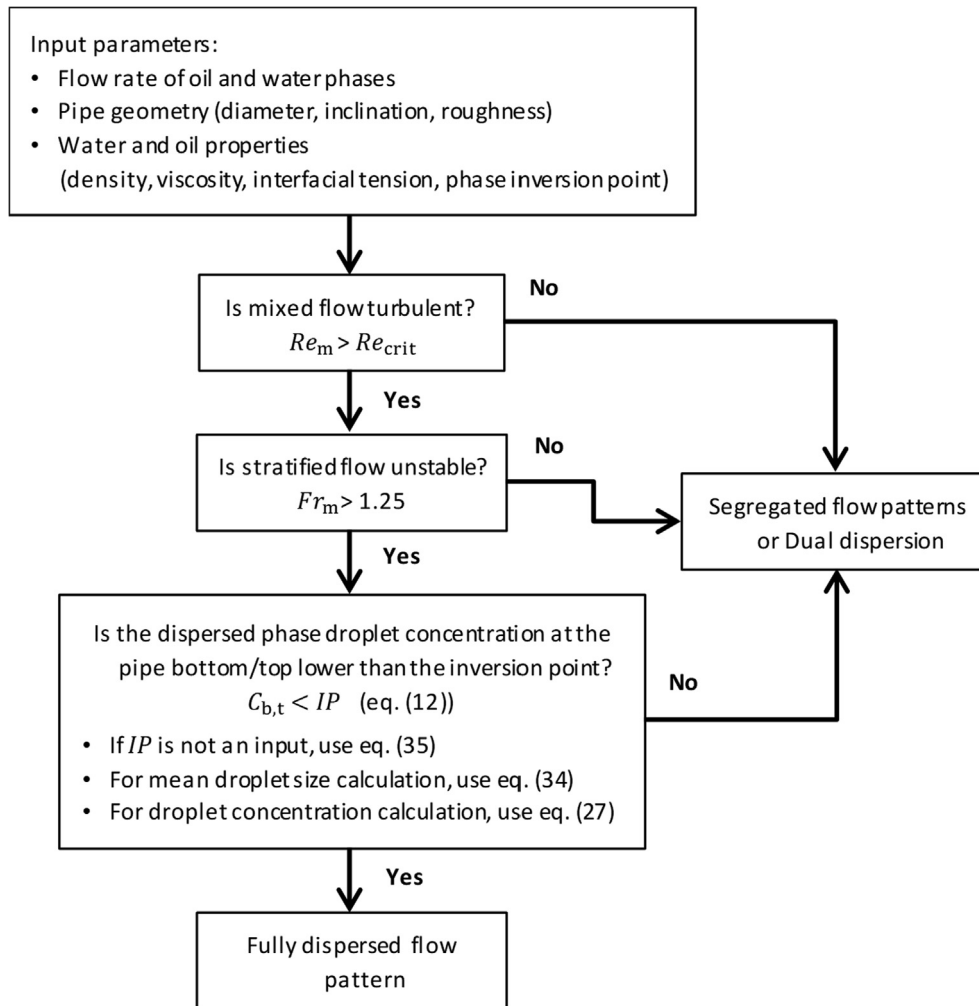


Fig. 17. Model flow chart.

and segregation via reaching critical concentrations that can be associated with the phase inversion point of the liquid-liquid mixture; which is an important parameter that is usually neglected by most of the available models.

The mechanistic nature of the model allows predicting dispersed flow transition bounds in a wide range of fluid physical properties and flow rates, pipe diameters and inclinations. In addition, the model can be easily implemented with very little numerical effort.

The prediction of critical mixture velocities for fully dispersed flow using the phase inversion point as critical dispersed phase concentration ( $C_{b,t} < IP$ ) have been compared with extensive sets of quality experimental data from numerous authors, showing a very good agreement in horizontal and inclined flows of mineral oil and water, as well as flows of crude oil and water. Moreover, these predicted transition bounds for fully dispersed flow have been proven to be more accurate and descriptive than predictions from the commonly used criteria by Brauner; particularly, for low dispersed phase volume fractions (e.g., <5%) and dispersed volume fractions near to the phase inversion point.

## 5. Notations

A cross sectional area of the pipe,  $m^2$   
 C droplet volumetric concentration, dimensionless

$C_{b,t}$  droplet volumetric concentration at the bottom or the top of the pipe, dimensionless  
 $C_{crit}$  critical droplet volumetric concentration, dimensionless  
 $C_D$  droplet drag coefficient, dimensionless  
 $C_{\epsilon_d}$  parameter to calculate droplet sizes in dense dispersions, dimensionless  
 $C_H$  constant to calculate droplet sizes in dense dispersions (Brauner), dimensionless  
 $D$  pipe diameter, m  
 $d$  droplet size, m  
 $d_{crit}$  critical droplet diameter, m  
 $d_{cb}$  critical droplet diameter from buoyancy criterion, m  
 $d_{c\sigma}$  critical droplet diameter from deformation criterion, m  
 $d_{max}$  maximum droplet diameter, m  
 $d_{max,o}$  maximum droplet diameter in dilute dispersion, m  
 $d_{max,\epsilon_d}$  maximum droplet diameter in dense dispersion (Brauner), dimensionless  
 $\bar{d}$  mean droplet diameter, m  
 $e_r$  equivalent sand roughness of the internal pipe wall, m  
 $f$  Fanning friction factor, dimensionless  
 $F_g$  gravity force on dispersed droplets, N  
 $F_t$  radial turbulent drag force on dispersed droplets, N  
 $Fr_m$  Froude number of the mixture flow, dimensionless  
 $g$  gravitational acceleration,  $m/s^2$   
 $IP$  phase inversion point, dimensionless  
 $I_1(K)$  modified Bessel function of order 1, dimensionless  
 $K$  parameter,  $DU_{s,y}/2\epsilon$ , dimensionless

|           |   |
|-----------|---|
| $l$       | pipe length, m  |
| $l_s$     | length scale for the attainment of the droplet settling velocity, m   |
| $Re_c$    | Reynolds number based on the continuous phase flow, dimensionless     |
| $Re_m$    | Reynolds number of the mixture flow, dimensionless                    |
| $Re_p$    | Reynolds number of a settling droplet, dimensionless                  |
| $U_c$     | continuous phase velocity, m/s  |
| $U_d$     | dispersed phase velocity, m/s   |
| $U_m$     | mixture velocity, m/s   |
| $U_s$     | droplet settling velocity, m/s  |
| $U_{s,y}$ | Component of the droplet settling velocity in the direction $y$ , m/s |
| $U_{sc}$  | superficial velocity of the continuous phase, m/s                     |
| $U_{sd}$  | superficial velocity of the dispersed phase, m/s                      |
| $u^*$     | friction velocity, m/s  |
| $v'$      | radial turbulent velocity fluctuations, m/s                           |
| $y$       | vertical coordinate respect to the pipe axis, m                       |

#### Greek letters

|                   |  |
|-------------------|--|
| $\beta$           | pipe inclination angle from the horizontal, radians                            |
| $\varepsilon$     | droplet turbulent diffusivity, $m^2/s$   |
| $\varepsilon_d$   | mean volumetric fraction of dispersed phase, dimensionless                     |
| $\varepsilon_w$   | mean volumetric fraction of water (water cut), dimensionless                   |
| $\varepsilon_w^l$ | water volumetric fraction for phase inversion, dimensionless                   |
| $\epsilon$        | mean energy dissipation rate per unit of mass of the continuous phase, Watt/kg |
| $\zeta$           | dimensionless eddy diffusivity, dimensionless                                  |
| $\mu_c$           | continuous phase viscosity, Pa.s   |
| $\mu_d$           | dispersed phase viscosity, Pa.s  |
| $\mu_o$           | oil viscosity, Pa.s  |
| $\mu_m$           | mixture viscosity, Pa.s  |
| $\mu_w$           | water viscosity, Pa.s  |
| $\mu$             | ratio $\mu_o/\mu_w$ , dimensionless  |
| $\rho_c$          | continuous phase density, $kg/m^3$   |
| $\rho_d$          | dispersed phase density, $kg/m^3$  |
| $\rho_o$          | oil density, $kg/m^3$  |
| $\rho_m$          | mixture density, $kg/m^3$  |
| $\rho_w$          | water density, $kg/m^3$  |
| $\rho$            | ratio $\rho_o/\rho_w$ , dimensionless  |
| $\sigma$          | interfacial liquid-liquid tension, N/m   |

#### Declaration of Competing Interest

The authors declare that they have no known competing financial interests or personal relationships that could have appeared to influence the work reported in this paper.

#### Acknowledgments

The author wants to thank BP, ConocoPhillips, Enbridge, Exxon-Mobil, Petronas, Total and Shell for their financial support to the Water Wetting JIP held at the Institute for Corrosion and Multiphase Technology. Helpful comments of Dr. Bert Pots and Dr. Marc Singer are also greatly appreciated.

#### References

- Al-Sarkhi, A., Pereyra, E., Mantilla, I., Avila, C., 2017. Dimensionless oil-water stratified to non-stratified flow pattern transition. *Journal of Petroleum Science and Engineering* 151, 284–291.
- Al-Wahaibi, T., Angeli, P., 2007. Transition between stratified and non-stratified horizontal oil–water flows. Part I: Stability analysis. *Chemical Engineering Science* 62, 2915–2928.
- Alkaya, B., Jayawardena, S.S., Brill, J.P., 2000. Oil–Water Flow Patterns in Slightly Inclined Pipes, ETCE/OMAE Joint Conference. ASME, New Orleans, LA, 775–782.
- Amundsen, L., 2011. An experimental study of oil–water flow in horizontal and inclined pipes. PhD thesis, Department of Energy and Process Engineering, Norwegian University of Science and Technology, Trondheim.
- Angeli, P., Hewitt, G.F., 1999. Pressure gradient in horizontal liquid–liquid flows. *International Journal of Multiphase Flow* 24, 1183–1203.
- Angeli, P., Hewitt, G.F., 2000a. Drop size distributions in horizontal oil–water dispersed flows. *Chemical Engineering Science* 55, 3133–3143.
- Angeli, P., Hewitt, G.F., 2000b. Flow structure in horizontal oil–water flow. *International Journal of Multiphase Flow* 26, 1117–1140.
- Arashmid, M., Jeffreys, G.V., 1980. Analysis of the phase inversion characteristics of liquid–liquid dispersions. *AIChE Journal* 26, 51–55.
- Arirachakaran, S., Oglesby, K.D., Malinowsky, M.S., Shohan, O., Brill, J.P., 1989. An Analysis of Oil/Water Flow Phenomena in Horizontal Pipes, SPE Production Operations Symposium. SPE, Oklahoma, OK, SPE-18836-MS.
- Barnea, D., 1987. A unified model for predicting flow–pattern transitions for the whole range of pipe inclinations. *International Journal of Multiphase Flow* 13, 1–12.
- Brauner, N., 2001. The prediction of dispersed flows boundaries in liquid–liquid and gas–liquid systems. *International Journal of Multiphase Flow* 27, 885–910.
- Brauner, N., Moalem Maron, D., 1992. Stability analysis of stratified liquid–liquid flow. *International Journal of Multiphase Flow* 18, 103–121.
- Brauner, N., Ullmann, A., 2002. Modeling of phase inversion phenomenon in two-phase pipe flows. *International Journal of Multiphase Flow* 28, 1177–1204.
- Brinkman, H.C., 1952. The Viscosity of Concentrated Suspensions and Solutions. *The Journal of Chemical Physics* 20, 571.
- Brodkey, R.S., 1967. *The Phenomena of Fluid Motions*. Dover Publications, INC., New York.
- Crowe, C.T., 2000. On models for turbulence modulation in fluid–particle flows. *International Journal of Multiphase Flow* 26, 719–727.
- Elseth, G., 2001. An Experimental Study of Oil / Water Flow in Horizontal Pipes, Department of Technology PhD Thesis. The Norwegian. University of Science and Technology, Porsgrunn.
- Feng, Z.-G., Michaelides, E.E., 2001. Drag Coefficients of Viscous Spheres at Intermediate and High Reynolds Numbers. *Journal of Fluids Engineering* 123, 841–849.
- Flores, J.G., 1997. Oil-Water Flow in Vertical and Deviated Wells. PhD thesis. The University of Tulsa, Tulsa OK.
- Haaland, S.E., 1983. Simple and Explicit Formulas for the Friction Factor in Turbulent Pipe Flow. *Journal of Fluids Engineering* 105, 89–90.
- Hinze, J.O., 1955. Fundamentals of the hydrodynamic mechanism of splitting in dispersion processes. *AIChE Journal* 1, 289–295.
- Ioannou, K., Nydal, O.J., Angeli, P., 2005. Phase inversion in dispersed liquid–liquid flows. *Experimental Thermal and Fluid Science* 29, 331–339.
- Karabelas, A.J., 1977. Vertical distribution of dilute suspensions in turbulent pipe flow. *AIChE Journal* 23, 426–434.
- Karabelas, A.J., 1978. Droplet size spectra generated in turbulent pipe flow of dilute liquid/liquid dispersions. *AIChE Journal* 24, 170–180.
- Kaushal, D.R., Tomita, Y., Dighade, R.R., 2002. Concentration at the pipe bottom at deposition velocity for transportation of commercial slurries through pipeline. *Powder Technology* 125, 89–101.
- Kostoglou, M., Karabelas, A.J., 2005. Toward a unified framework for the derivation of breakage functions based on the statistical theory of turbulence. *Chemical Engineering Science* 60, 6584–6595.
- Kroes, R., Amundsen, L., Hoffmann, R., 2013. Crude oil–water flow in horizontal pipes, Internship Report MSc thesis. University of Twente, Twente.
- Kubie, J., Gardner, G.C., 1977. Drop sizes and drop dispersion in straight horizontal tubes and in helical coils. *Chemical Engineering Science* 32, 195–202.
- Kumara, W.A.S., Halvorsen, B.M., Melaaen, M.C., 2009. Pressure drop, flow pattern and local water volume fraction measurements of oil–water flow in pipes. *Measurement Science and Technology* 20, 114004.
- Liao, Y., Lucas, D., 2010. A literature review on mechanisms and models for the coalescence process of fluid particles. *Chemical Engineering Science* 65, 2851–2864.
- Lovick, J., Angeli, P., 2004. Experimental studies on the dual continuous flow pattern in oil–water flows. *International Journal of Multiphase Flow* 30, 139–157.
- Lovick, J., Mouza, A., Paras, S., Lye, G., Angeli, P., 2005. Drop size distribution in highly concentrated liquid–liquid dispersions using a light back scattering method. *Journal of Chemical Technology & Biotechnology* 80, 545–552.
- Lum, J.Y.L., Al-Wahaibi, T., Angeli, P., 2006. Upward and downward inclination oil–water flows. *International Journal of Multiphase Flow* 32, 413–435.
- Mlynek, Y., Resnick, W., 1972. Drop sizes in an agitated liquid–liquid system. *AIChE Journal* 18, 122–127.
- Mukherjee, H., Brill, J.P., Beggs, H.D., 1981. Experimental Study of Oil–Water Flow in Inclined Pipes. *Journal of Energy Resources Technology* 103, 56–66.
- NACE, 2008. SP0208-2008. Internal Corrosion Direct Assessment Methodology for Liquid Petroleum Pipelines, NACE, Houston TX.
- Nädler, M., Mewes, D., 1997. Flow induced emulsification in the flow of two immiscible liquids in horizontal pipes. *International Journal of Multiphase Flow* 23, 55–68.
- Pal, R., 1996. Effect of droplet size on the rheology of emulsions. *AIChE Journal* 42, 3181–3190.
- Paolinelli, L.D., Rashedi, A., Yao, J., Singer, M., 2018. Study of water wetting and water layer thickness in oil–water flow in horizontal pipes with different wettability. *Chemical Engineering Science* 183, 200–214.

- Piela, K., Delfos, R., Ooms, G., Westerweel, J., Oliemans, R.V.A., 2008. On the phase inversion process in an oil–water pipe flow. *International Journal of Multiphase Flow* 34, 665–677.
- Plasencia, J., Pettersen, B., Nydal, O.J., 2013. Pipe flow of water-in-crude oil emulsions: Effective viscosity, inversion point and droplet size distribution. *Journal of Petroleum Science and Engineering* 101, 35–43.
- Pots, B.F.M., Hollenberg, J.F., Hendriksen, E.L.J.A., 2006. What are the Real Influences of Flow on Corrosion?, NACE Corrosion 2006. NACE, Houston, TX, Paper 6591.
- Richardson, J.F., Zaki, W.N., 1997. Sedimentation and fluidisation: Part I. *Chemical Engineering Research and Design* 75, S82–S100.
- Rivkind, V.Y., Ryskin, G.M., 1976. Flow structure in motion of a spherical drop in a fluid medium at intermediate Reynolds numbers. *Fluid Dynamics* 11, 5–12.
- Rodriguez, O.M.H., Oliemans, R.V.A., 2006. Experimental study on oil–water flow in horizontal and slightly inclined pipes. *International Journal of Multiphase Flow* 32, 323–343.
- Saffman, P.G., 1965. The lift on a small sphere in a slow shear flow. *Journal of Fluid Mechanics* 22, 385–400.
- Sarica, C., Zhang, H.Q., 2008. Development of Next Generation Multiphase Pipe Flow Prediction Tools. United States Department of Energy. University of Tulsa, Tulsa OK.
- Schiller, L., Naumann, A., 1933. *Über die grundlegenden Berechnungen bei der Schwerkraftaufbereitung*. Zeitschrift des Vereines Deutscher Ingenieure 77, 318–320.
- Segev, A., 1984. Mechanistic Model for Estimating Water Dispersion in Crude Oil Flow. Annual AIChE Meeting, AIChE, San Francisco, CA, Paper, p. 124a.
- Selker, A.H., Sleicher Jr., C.A., 1965. Factors affecting which phase will disperse when immiscible liquids are stirred together. *The Canadian Journal of Chemical Engineering* 43, 298–301.
- Sharma, A., Al-Sarkhi, A., Sarica, C., Zhang, H.-Q., 2011. Modeling of oil–water flow using energy minimization concept. *International Journal of Multiphase Flow* 37, 326–335.
- Simmons, M.J.H., Azzopardi, B.J., 2001. Drop size distributions in dispersed liquid–liquid pipe flow. *International Journal of Multiphase Flow* 27, 843–859.
- Torres, C.F., Mohan, R.S., Gomez, L.E., Shoham, O., 2015. Oil-Water Flow Pattern Transition Prediction in Horizontal Pipes. *Journal of Energy Resources Technology* 138, 022904–022911.
- Trallero, J.L., 1995. Oil-Water Flow Patterns in Horizontal Pipes. PhD Thesis. University of Tulsa, Tulsa, OK.
- Valle, A., 2000. Three phase gas-oil-water pipe flow. PhD Thesis. Department of Chemical Engineering and Chemical Technology. Imperial College of Science, Technology and Medicine, London.
- Vielma, M.A., Atmaca, S., Sarica, C., Zhang, H.-Q., 2008. Characterization of Oil/water Flows in Horizontal Pipes. *SPE Proj. Facil. Constr.* 3, 1–21.
- Vigneaux, P., Chenais, P., Hulin, J.P., 1988. Liquid-liquid flows in an inclined pipe. *AIChE J.* 34, 781–789.
- Wang, C.Y., Calabrese, R.V., 1986. Drop breakup in turbulent stirred-tank contactors. Part II: Relative influence of viscosity and interfacial tension. *AIChE J.* 32, 667–676.
- Wang, Z., Zhang, Q., Zeng, Q., Wei, J., 2017. A unified model of oil/water two-phase flow in the horizontal wellbore. *SPE J.* 22, 353–364.
- Zavareh, F., Hill, A.D., Podio, A., 1988. Flow Regimes in Vertical and Inclined Oil/Water Flow in Pipes, in: SPE Annual Technical Conference and Exhibition. SPE, Houston, TX, SPE-18215-MS.
- Zhai, L.-S., Jin, N.-D., Zong, Y.-B., Hao, Q.-Y., Gao, Z.-K., 2015. Experimental flow pattern map, slippage and time–frequency representation of oil–water two-phase flow in horizontal small diameter pipes. *Int. J. Multiphase Flow* 76, 168–186.
- Zhang, H.-Q., Sarica, C., 2006. Unified modeling of gas/oil/water pipe flow – basic approaches and preliminary validation. *SPE Proj. Facil. Constr.* 1, 1–7.
- Zhang, H.-Q., Wang, Q., Sarica, C., Brill, J.P., 2003. A unified mechanistic model for slug liquid holdup and transition between slug and dispersed bubble flows. *Int. J. Multiphase Flow* 29, 97–107.